EJN European Journal of Neuroscience

FENS Federation of European Neuroscience Societies

European Journal of Neuroscience, Vol. 42, pp. 2934–2951, 2015 doi:10.1111/ejn.13093

COGNITIVE NEUROSCIENCE

Spatial transformations between superior colliculus visual and motor response fields during head-unrestrained gaze shifts

Morteza Sadeh,[1,2,3,4] Amirsaman Sajad,[1,2,3,4] Hongying Wang,[1,3,4] Xiaogang Yan[1,3,4] and John Douglas Crawford[1,2,3,4]

[1]York Centre for Vision Research, Room 0009A LAS, 4700 Keele Street, Toronto, ON, M3J 1P3, Canada
[2]York Neuroscience Graduate Diploma Program, Toronto, ON, Canada
[3]Canadian Action and Perception Network (CAPnet), York University, Toronto, ON, Canada
[4]Departments of Psychology, Biology, and Kinesiology and Health Science, York University, Toronto, ON, Canada

Keywords: eye movement, gaze control, head movement, monkeys, unit recording, visuomotor transformation

Edited by Doug Munoz
Received 6 December 2014, revised 14 September 2015, accepted 30 September 2015

Abstract

We previously reported that visuomotor activity in the superior colliculus (SC) – a key midbrain structure for the generation of rapid eye movements – preferentially encodes target position relative to the eye (Te) during low-latency head-unrestrained gaze shifts (DeSouza *et al.*, 2011). Here, we trained two monkeys to perform head-unrestrained gaze shifts after a variable post-stimulus delay (400–700 ms), to test whether temporally separated SC visual and motor responses show different spatial codes. Target positions, final gaze positions and various frames of reference (eye, head, and space) were dissociated through natural (untrained) trial-to-trial variations in behaviour. 3D eye and head orientations were recorded, and 2D response field data were fitted against multiple models by use of a statistical method reported previously (Keith *et al.*, 2009). Of 60 neurons, 17 showed a visual response, 12 showed a motor response, and 31 showed both visual and motor responses. The combined visual response field population ($n = 48$) showed a significant preference for Te, which was also preferred in each visual subpopulation. In contrast, the motor response field population ($n = 43$) showed a preference for final (relative to initial) gaze position models, and the Te model was statistically eliminated in the motor-only population. There was also a significant shift of coding from the visual to motor response within visuomotor neurons. These data confirm that SC response fields are gaze-centred, and show a target-to-gaze transformation between visual and motor responses. Thus, visuomotor transformations can occur between, and even within, neurons within a single frame of reference and brain structure.

Introduction

The superior colliculus (SC) is involved in the transformation of visual signals into motor commands for gaze shifts (Wurtz & Albano, 1980; Sparks & Hartwich-Young, 1989; Sparks & Mays, 1990; Everling *et al.*, 1999a,b; Sparks, 2002; Gandhi & Katnani, 2011). Neurons in the superficial and intermediate layers respond to visual stimuli (visual neurons), whereas the intermediate and deep layers also (or only) show saccade-related activity (visuomotor and motor neurons) (Wurtz & Goldberg, 1971, 1972a,b; Cynader & Berman, 1972; Goldberg & Wurtz, 1972a; Sparks, 1975, 1978; Schiller, 1977; Munoz & Wurtz, 1995). These layers form closely aligned topographic visual and motor maps (Sparks, 1986, 1988; Marino *et al.*, 2008), and many individual cells show congruent visual and motor response fields (RFs) (Sparks & Hartwich-Young, 1989; Hartwich-Young *et al.*, 1990; Marino *et al.*, 2008). However, none of these factors (i.e. temporal segregation of visual and motor responses, topography, or RF structure) directly show which spatial parameters (i.e. stimulus location, vs. gaze eye or head movement parameters, in various frames of reference) are encoded within SC activity.

This is the question addressed in the current study, specifically: what spatial parameters are encoded within SC visual and motor bursts during head-unrestrained gaze shifts in response to remembered visual stimuli, and how are these signals transformed through different identified cell types? On the basis of SC physiology and anatomy, one might expect visual responses (in visual and visuomotor cells) to encode the location of a target relative to the eye, like the retina (Cynader & Berman, 1972; Marrocco & Li, 1977; Berson, 1988; Snyder, 2000), but motor responses (in visuomotor and motor cells) might encode a variety of different spatial parameters. Motor responses might still encode stimulus location (Sparks, 1989; Stanford & Sparks, 1994; Frens & Van Opstal, 1997; Edelman & Goldberg, 2002; Quessy *et al.*, 2010), or they might encode movement direction (Everling *et al.*, 1999a,b). If they encode movement direc-

Correspondence: J. D. Crawford, [1]York Centre for Vision Research, as above.
E-mail: jdc@yorku.ca

tion, they might encode eye + head gaze displacement (Munoz *et al.*, 1991a,b; Freedman & Sparks, 1997b), or they might show separate eye and head signals (Cowie & Robinson, 1994; Cowie *et al.*, 1994; Walton *et al.*, 2007; Rezvani & Corneil, 2008; Nagy & Corneil, 2010; Monteon *et al.*, 2012). Finally, gaze, eye or head commands must be defined in some frame of reference (Crawford *et al.*, 2011). Some early studies suggested that space-fixed goals are encoded in the posterior SC (Guitton *et al.*, 1980; Roucoux *et al.*, 1980; McIlwain, 1986), but since then most head-unrestrained studies (Sparks, 1978, 1989; Van Opstal *et al.*, 1991; Lee & Groh, 2012) and head-unrestrained studies (Freedman & Sparks, 1997a,b; Klier *et al.*, 2001; Choi & Guitton, 2009; DeSouza *et al.*, 2011) have emphasized eye-centred codes.

To our knowledge, no previous study has established the difference in spatial coding between SC visual and motor RFs in head-unrestrained conditions. This is particularly difficult to address, because target, gaze, eye and head motion tend to co-vary, and 3D eye and head orientations are too variable (torsionally, vertically, and horizontally) for a conventional reference frame analysis. However, we recently developed a way to test between all of the possibilities listed in the preceding paragraph, simply by mapping visual and motor RFs relative to different gaze parameters, and then determining which 'model' leaves the least residuals in the variability of neural responses for a particular point in that space (Keith *et al.*, 2009). We previously used this method to show that the SC population RFs are primarily organized according to target location relative to initial eye orientation during gaze saccades made immediately to visual targets (DeSouza *et al.*, 2011). Here, we probed SC physiology more deeply through the use of improved task parameters, additional models (for gaze, vs. eye, vs. head motion), and, most importantly, a memory-delay paradigm that allowed us to discriminate visual and motor responses, and trace their spatial codes through visual, visuomotor and motor cells (Sajad *et al.*, 2014).

Materials and methods

Surgical procedures for neurophysiological and behavioural recordings

The data were collected from two female *Macaca mulatta* monkeys (M1 and M2; age, 10 years; weights, 6.5 and 7 kg) with a protocol approved by the York University Animal Care Committee in accordance with guidelines published by the Canadian Council for Animal Care. With surgical procedures described previously (Crawford *et al.*, 1999; Klier *et al.*, 2001, 2003a,b), the monkeys were prepared for long-term electrophysiology and 3D gaze movement recordings. Each monkey was subjected to general anaesthesia with 1–2% isoflurane after intramuscular injection of ketamine hydrochloride (10 mg/kg), atropine sulphate (0.05 mg/kg), and acepromazine (0.5 mg/kg). During the surgery, we implanted a vertically aligned unit recording chamber (i.e. with no tilt) placed 5 mm anterior and 0 mm lateral in stereotaxic coordinates, which allowed access to the left and right SC. This chamber angle and position were chosen to minimize collisions between the electrode/microdrive and the experimental setup during head movements, and to simplify the use of stereotaxic coordinates during recordings. The chamber was then surrounded by a dental acrylic cap, which was anchored to the skull with 13 stainless steel cortex screws. Two scleral search coils (diameter, 5 mm) were implanted in one eye of the monkeys to record 3D eye movements. Two orthogonal coils, which were secured with a screw on a plastic base on the cap, recorded the 3D head movements during the experiments. 3D recordings and analysis were performed as described previously (Crawford *et al.*, 1999; DeSouza *et al.*, 2011).

Experimental equipment

We used a Pentium IV PC and custom-designed software to present stimuli, control behaviour paradigms, send digital codes to a Plexon data acquisition system, and deliver juice rewards to the monkeys. Stimuli were presented on a screen 60 cm in front of the monkey, by use of a projector (WT600 DLP projector; NEC). Monkeys were seated on a custom-designed primate chair in order to have their heads move freely at the centre of a 1-m^3 magnetic field generator (Crawford *et al.*, 1999), and a juice spout (Crist Instruments) was placed on the skull cap for computer-controlled delivery of the juice reward to the monkey's mouth.

Behavioural paradigm

In order to separate visual and motor responses, monkeys were trained to perform memory-guided gaze shifts. First, they looked at a fixation point near the centre of the screen, which was a green circle with a radius of 0.5°. The fixation light remained on for another 400–700 ms, in order to introduce a variable memory delay and discourage anticipation of the go signal, which was the disappearance of the initial fixation point. After 300 ms, a target stimulus appeared (red circle with a size of 0.5°) in the periphery for 125 ms. When the go signal was presented, the monkeys made a gaze shift towards the remembered location of the target, and were required to maintain fixation for at least 200 ms at that final position to obtain the juice reward. The fixation light remained on for another 400–700 ms in order to introduce a variable memory delay and discourage anticipation of the go signal. The proper maintenance of initial fixation was ensured by setting a tolerance window of 2–4° (radius) with respect to the fixation position. In order to spatially separate targets vs. gaze coding, we allowed a tolerance window of diameter 6–12° for gaze errors around the remembered locations of the targets, and thus allowed monkeys to produce a natural (i.e. self-selected) distribution of gaze end points around the targets (Fig. 1).

For our analytical method to work (see 'Model fitting' below), we needed to: (i) span the spatially modulated portion of each neuron's RF through a proper distribution of visual targets and eye–head gaze shifts; and (ii) have trial-to-trial variations between different gaze parameters (target vs. gaze, gaze vs. to head, different frames, etc.). The first requirement was accomplished through placement of targets that evoked activity throughout the RF, and the second through natural (untrained) variations in behaviour.

During experiments, the target stimuli were presented in the visual field contralateral to the hemifield of the recording site (see 'Neural recordings'). Once a neuron had been isolated, the RFs were estimated through initial mapping, which involved monkeys performing visually guided saccades to a wide range of stimuli presented on the screen while cell activity was monitored on-line. Test stimuli were then selected within a grid (12–32 targets, depending on the RF size) that extended just beyond the cell's receptive field. During testing, stimuli were presented in a randomized order, and each target was presented for at least seven successful gaze shifts. The initial fixating point was varied randomly from one trial to another within a square range approximately equal to the cell's RF size (Fig. 1). This variation led to greater variation in initial 3D gaze, head and eye positions (Fig. 2A–F) than in DeSouza *et al.* (2011). This was important for distinguishing different reference frames (see 'Model fitting').

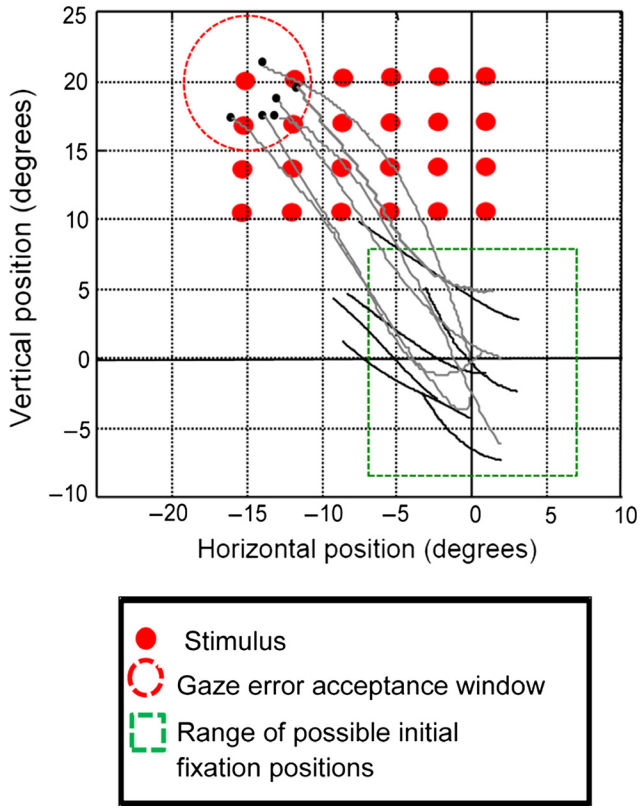

FIG. 1. Example stimulus (red circles) locations and gaze/head trajectories. For this example, the red circle at the top left corner was the target. Other possible targets for other trials are also shown, but were not presented at the same time. The initial fixation position was randomly varied within a range approximately similar to the RF of the isolated neuron (green square). Gaze errors were tolerated (i.e. rewarded) if the gaze landed within a certain distance from the target (6–12° range for all experiments, and 8° in this example). The head and gaze trajectories towards the example stimulus are also indicated, by black and grey lines respectively. The variations in the initial positions of gaze and head relative to the centre of the screen were utilized to dissociate eye, head and space coordinates, and helped to encourage different eye and head trajectory amplitudes and directions for different gaze shifts to a given target (see Materials and methods).

Otherwise, the monkeys were allowed to vary initial combinations of 3D eye and head orientations (Fig. 2, left and centre columns) and the relative amounts of eye and head contributions to the gaze shift (Fig. 2, right column) as they wished (this was important for distinguishing different target, gaze, eye and head models). Example variations between final gaze position and head position relative to one target are shown in Fig. 1. The right columns of Fig. 2G–I show example distributions of gaze, head and eye amplitudes (vertical; up the end of the gaze shift) for one RF-mapping experiment, and Fig. 3A shows the corresponding 'full head' movement (defined as the end point of motion or the largest excursion point of the head before it returned). Figure 3B and C shows the full distribution of gaze, head (to end of gaze) and full head movements for all experiments in both monkeys, with corresponding statistics in the figure legend. Note that many of the head movements are small, but, for our method, this does not matter, so long as: (i) they were the movements that corresponded to our RF mapping; and (ii) they showed trial-to-trial variability relative to the other gaze parameters. This is illustrated in the right column of Fig. 3, where Fig. 3D shows colour-coded examples of variations in head movement associated with three targets, and Fig. 3E and F quantify this across all trials for each monkey by plotting the standard deviation of gaze and head amplitudes for each target location, as a function of target distance from the centre. This shows that there is variability in both these parameters throughout the range that we explored, although it scales to movement size in both parameters. Thus, RF maps based on head movement would be spatially compressed relative to target-based or gaze-based RFs, but this is accounted for in our non-parametric analysis method (Keith & Crawford, 2008).

As a result of these simple manipulations and the naturally variable behaviour produced by the monkeys, every neuron that we report below was tested with a variety of initial 3D eye and head orientations, final target positions, final gaze positions, and different combinations of relative eye and head motion during the gaze shift. This provided the behavioural basis for the spatial separation between the models described below.

Trial definition and inclusion criteria

The beginning of a trial was marked by the appearance of the initial fixation point. The beginning of the gaze saccade was defined as the instant when its velocity exceeded 50°/s, and its end when its velocity decreased to 30°/s. The contribution of the head movement to gaze is defined here as the head movement from the start to the end of the gaze saccade. However, the head movement was often prolonged after the saccadic component of the gaze shift. Head movements were marked from the start of gaze movement until the point at which the head velocity decreased to below 15°/s. For trials in which the head velocity never exceeded 15°/s, the head position was sampled at the time of gaze onset and offset. The head movement marks were then visually inspected to ensure correct marks. For analysis, all trials were considered for analysis irrespective of whether or not the monkey received a reward after the trial. We excluded trials on the basis of spatial and temporal criteria. First, trials in which the directions of the gaze shifts were completely unrelated to the direction of the target (e.g. opposite direction) were removed. Then, we obtained the regression between errors in gaze vs. retinal error (note: retinal error is the retinal angle between the fovea and the target at the initial position before the gaze shift), and removed trials with gaze error two standard deviations greater than this regression line. Furthermore, every trial was visually inspected, and any trial in which the gaze shift was anticipated (reaction time of < 100 ms after the go signal), the gaze shift consisted of multi-step saccades or there was a saccade or head movement (> 5°) during the memory interval was excluded. The timing of the saccade was tightly linked to the time of the go signal, and was not influenced by the duration of the variable delay period: the correlation between the variable delay period and the reaction time of gaze shifts in response to the go signals was very low (0.11 for M1, $P = 0.62$; 0.012 for M2, $P = 0.24$). Finally, for each neuron, we required successful performance for at least 80% of total trials [mean ± standard error of the mean (SEM) trials = 162 ± 28], and at least seven successful gaze shifts towards each target location (with a possible maximum of 15, after excluding erroneous trials); also, the neuron had to remain isolated throughout the recording session.

Neural recordings

We recorded extracellular activity from the left and right SC with tungsten microelectrodes (FHC). The electrode was inserted through a guide tube, which was controlled by a hydraulic microdrive (MO-90S; Narishige International, East Meadow, NY, USA). Isolated

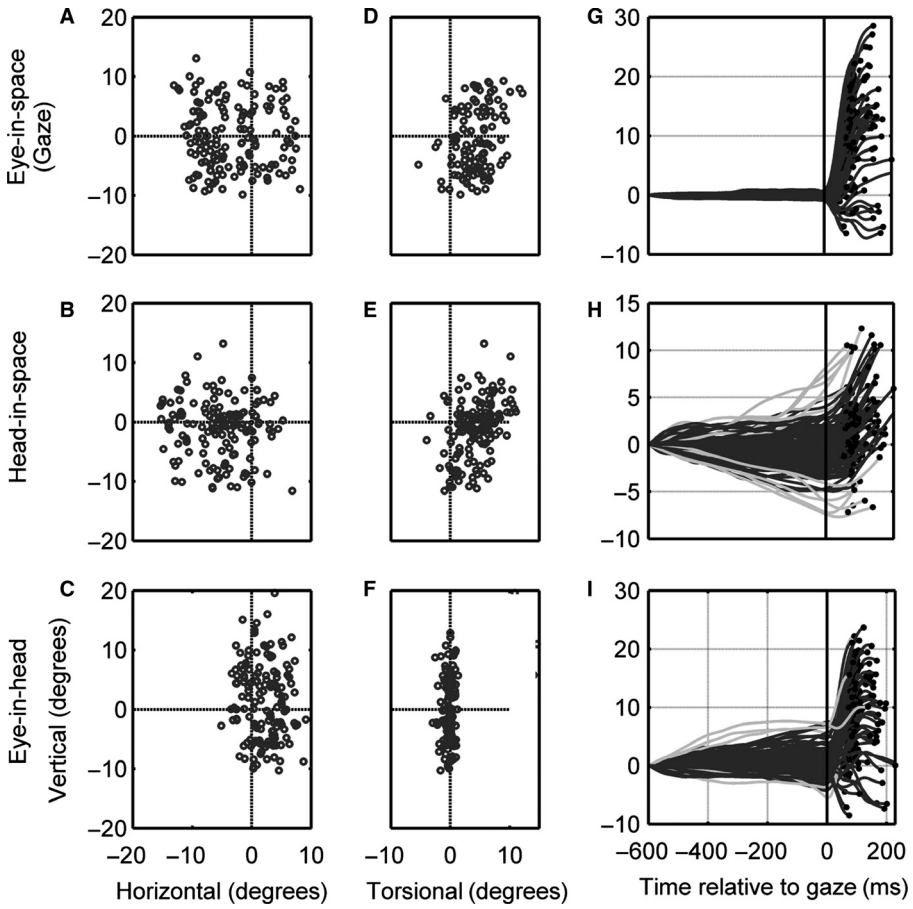

FIG. 2. Behavioural parameters used in our analysis. Horizontal and vertical variations in initial fixation position (circles) of gaze (A), head (B) and eye (C) along with the torsional components (D–F) are illustrated for the same experimental session as in Fig. 1. In the right column, the vertical component of gaze (G), head (H) and eye (I) movements are aligned with gaze onset, showing variability in amplitudes and in final vertical positions.

signals were amplified, filtered and stored for off-line sorting with the Plexon MAP system. The SC was identified according to criteria published previously (Klier *et al.*, 2001; DeSouza *et al.*, 2011). The process of identification included the following steps: (i) stereotaxic placement of the recording chamber; (ii) on-line calibration of the stereotaxic coordinates through recordings of additional small midbrain structures with highly characteristic firing patterns and 3D stimulation results, such as the interstitial nucleus of Cajal; (iii) advancement of electrodes in a search pattern based on the expected stereotaxic coordinates of the SC; (iv) a search for neural activity related to the presence of a visual stimulus and gaze onset, (v) preliminary on-line mapping of visual and motor RFs, and confirming that the observed RF followed the SC map; (vi) low-threshold, head-fixed microstimulation of sites (at the start and the end of the experiment) to confirm that saccades or staircase saccades with zero torsion were elicited; (vii) off-line analysis of results; and (viii) confirmation across experiments of the orderly rostrocaudal and mediolateral maps of RFs and stimulation-evoked movements characteristic of the SC. In addition, recording sites have now been histologically confirmed in one monkey. Cells that showed a clear response time-locked with the visual stimulus, saccade or both were recorded for off-line analysis.

Unit analysis and classification

After off-line spike sorting, neural activity was aligned with experimental events in order to classify the types of activity and neuron (Fig. 4). Visual neurons (Fig. 4B) were defined as cells that showed a robust burst of activity (> 50 spikes/s above the baseline) 40–60 ms after the stimulus presentation that lasted for ~180 ms afterwards (Goldberg & Wurtz, 1972a,b). Motor neurons (Fig. 4E) were those with robust activity or a buildup of activity peaking at the time of gaze onset, with activity starting prior to the gaze onset (100–40 ms before saccade), and that continued to ~100 ms after gaze onset. Neurons that met both of these criteria were classified as visuomotor (Fig. 4C and D). For visual neural activity, a fixed temporal analysis of 60–160 ms (with respect to target presentation) was used (Fig. 4B and C), and for motor neural activity a fixed temporal window of −50 ms to +50 ms (relative to gaze onset) was used (Fig. 4C and D). For this analysis, we only included head movement data up to the end of the gaze shift in our head-related model fits (see next section). We also analysed motor activity in a variable window that included the entire duration of the movement-related burst of each neuron. For this analysis, we included the entire head movement in our model fits (see below). When we refer to 'number of spikes' below, this refers to number of action potentials in these defined temporal windows.

Model fitting

We used a method previously reported by Keith *et al.* (2009) and DeSouza *et al.* (2011), with further optimization of the behavioural method for the analysis (Fig. 1) and the addition of effector-specific models, that is eye movement relative to the head and head

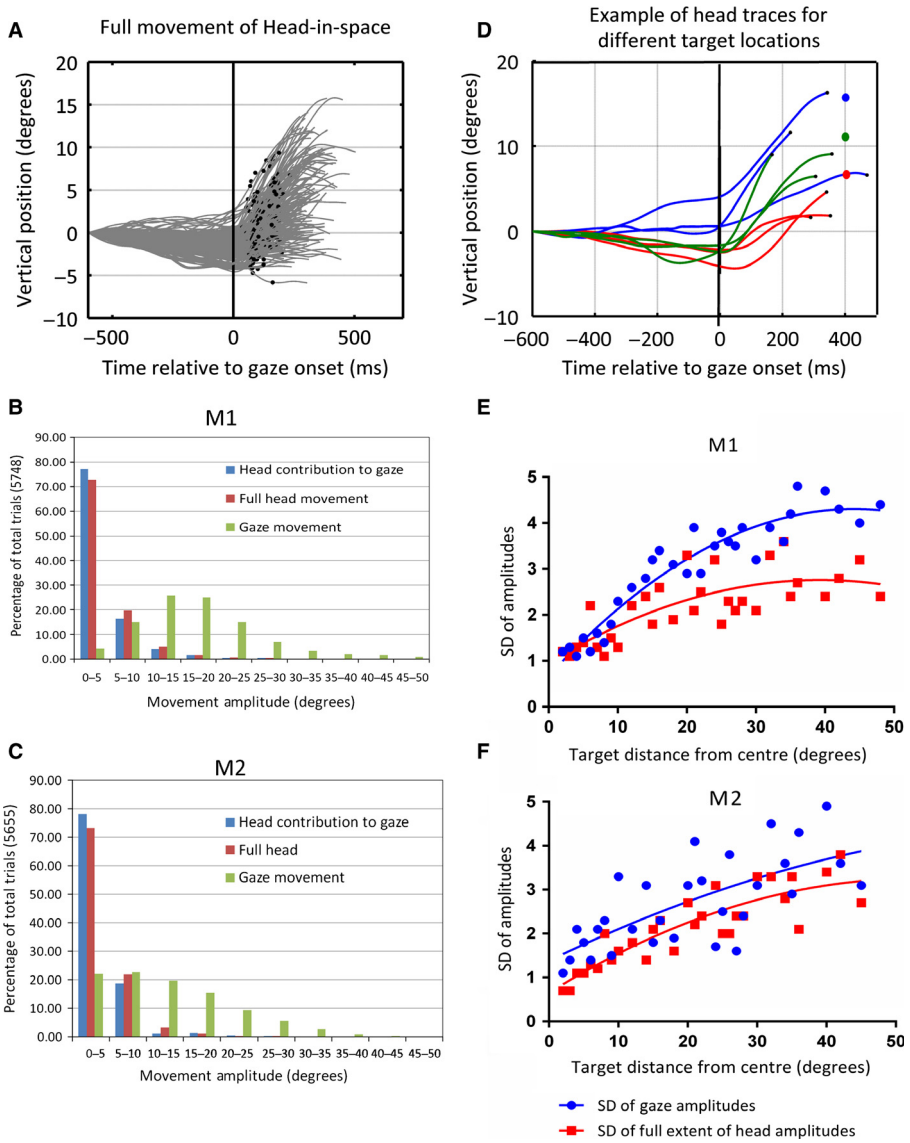

FIG. 3. Details of eye and head amplitudes in our dataset. (A) The vertical component of head movement is plotted as a function of time for the same trials as the one illustrated in Fig. 2H, but showing the head movement, with the point in time corresponding to the end of the first gaze shift indicated by the dark dots. (B) Frequency histogram for the complete distribution of gaze, (green), head contribution to gaze (blue) and full head movement (red) amplitudes for subject M1, across all experiments. For this monkey, the statistics for eye, head contribution to gaze and full head movement (respectively) in degrees were: mean amplitude (17.36, 1.86, 2.44), median amplitude (16.00, 0.90, 1.30), minimum amplitude (1.90, 0.00, 0.00), maximum amplitude (50.30, 43.30, 45.19), lower quartiles (11.20, 0.40, 0.52), and upper quartiles (21.40, 2.20, 2.86). (C). Same plot for subject M2. For this monkey, the statistics for eye, head contribution to gaze and full head movement (respectively) in degrees were: mean amplitude (12.85, 3.10, 4.37), median amplitude (11.10, 1.70, 2.64), minimum amplitude (1.70, 0.00, 0.00), maximum amplitude (49.50, 37.90, 45.48), lower quartile (5.50, 0.60, 1.32), and upper quartile (18.20, 4.10, 6.13). (D) Example plots of head movement as a function of time (selected from A), illustrating variability of amplitudes and end points relative to three different colour-matched targets (●). (E) Standard deviation (SD) of gaze (blue) and head (red) for each and every target position used with monkey M1, plotted as a function of target distance from the centre of the screen. (F) Same plot for monkey M2.

movement relative to space (Fig. 5). This approach allowed us to simultaneously test between different models without any special training (other than the delay fixation training), relying instead on the monkeys' natural variability in behaviour (Figs 1–3). In short, we plotted the RFs of neurons' visual and motor activity in various representations to identify the model that gave the most coherent fit, that is the least variability in number of spikes for a given spatial location, as illustrated schematically in Fig. 5B. Experimentally, this was quantified by use of the mean predictive sum of squares (PRESS) statistics. PRESS residuals were obtained by computing the residual for each trial relative to fits obtained from all of the other trials. The 'best fit' for the activity of a given neuron was defined as the smallest overall mean residual of the PRESS obtained from fits between numbers of spikes obtained from all trials, compared across all models, and across all bandwidths (the width of the convolution kernel used in fitting the data to each model). This method – as compared with traditional regression techniques – has the advantages that it makes no assumptions about the shape of the RF or linearity, and utilizes the full 2D range of the neural RF and 3D range of eye and head kinematics (Keith *et al.*, 2009; DeSouza *et al.*, 2011). These factors are all important in this study, because RFs in the SC are neither simple nor linear (e.g. Figs 7 and 9–11),

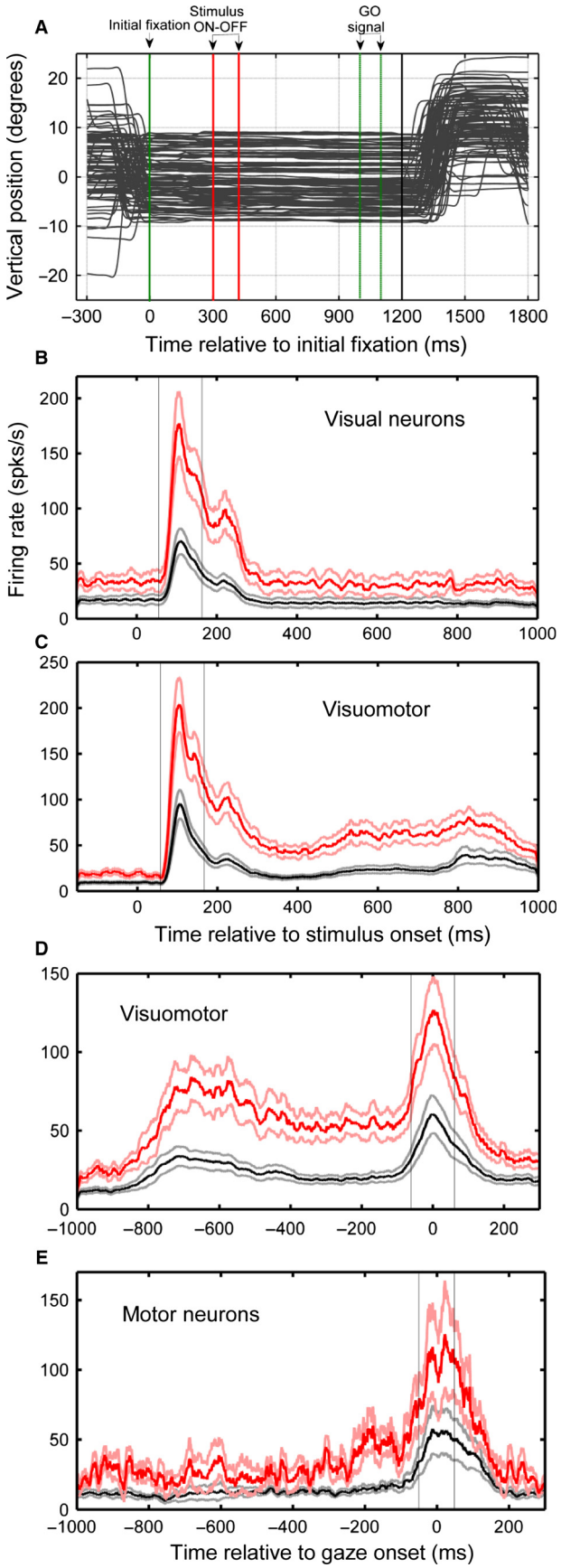

FIG. 4. Memory-guided saccade paradigm and population responses of visual, visuomotor and motor neurons. (A) Vertical eye positions aligned with different task events. The black vertical line after the gaze onset represents the reaction time gaze inclusion criteria (> 100 ms). (B) Spike density plot for visual neurons aligned with stimulus presentation. (C) Visual activity of visuomotor neurons aligned with stimulus presentation. (D) Motor activity of visuomotor neurons aligned with gaze onset. (E) Motor activity of motor neurons aligned with gaze onset. In B–E, the average number of spikes (± SEM) across all trials is shown in black, and the average number of spikes (± SEM) across 10% of trials with the highest firing rate (top 10% for each neuron) is shown in red with confidence intervals (light red). The sampling windows for visual (60–160 ms after stimulus onset) and motor (± 50 ms relative to gaze onset) responses are represented by vertical light grey lines.

and most of the models described below are inherently non-linear and/or depend on 3D eye or head orientation (Martinez-Trujillo *et al.*, 2003).

Here, we summarize all of the models included in our analysis (Fig. 5A).

Target models

In these models, we were testing whether neural activity encoded target location relative to initial 3D eye orientation (Te), target location relative to head orientation (Th), or in the space-fixed (or body-fixed) coordinates (Ts).

Gaze models

Here we tested whether neural activity encoded the final gaze position relative to initial eye orientation (Ge), the final gaze position relative to head orientation (Gh), or the final gaze position relative to space coordinates (Gs).

Displacement models

These models consider the possibility of neurons encoding the vector displacement (i.e. final position minus initial position) of the eye during gaze shifts (i.e. the saccade) (dE), gaze in space (i.e. gaze displacement vector as projected onto a 2D screen) (dG), or the head in space (dH).

Final eye and head position models

We tested models corresponding to the head's final position in space (Hs) or that of final eye position in the orbit (Eh) (note that some of these models may be quite similar spatially). For example, Ge and dG are both 'gaze-centred' in the sense that the zero reference position is initial gaze direction, but the coordinates of Ge are fixed in the eye, whereas the coordinates of dG are fixed in space (Crawford & Guitton, 1997). The difference between them only becomes evident for large deviations in eye orientation (torsion, vertical, or horizontal) combined with large gaze shift components in an orthogonal dimension (Klier *et al.*, 2001). Furthermore, both resemble dE when eye displacement dominates the gaze shift (Freedman & Sparks, 1997a,b).

We derived visual and/or motor RFs for each of our neurons for all of these models, by plotting the number of action potentials in our sampling windows (Fig. 4) for each trial as a function of the horizontal and vertical coordinates dictated by each of the above

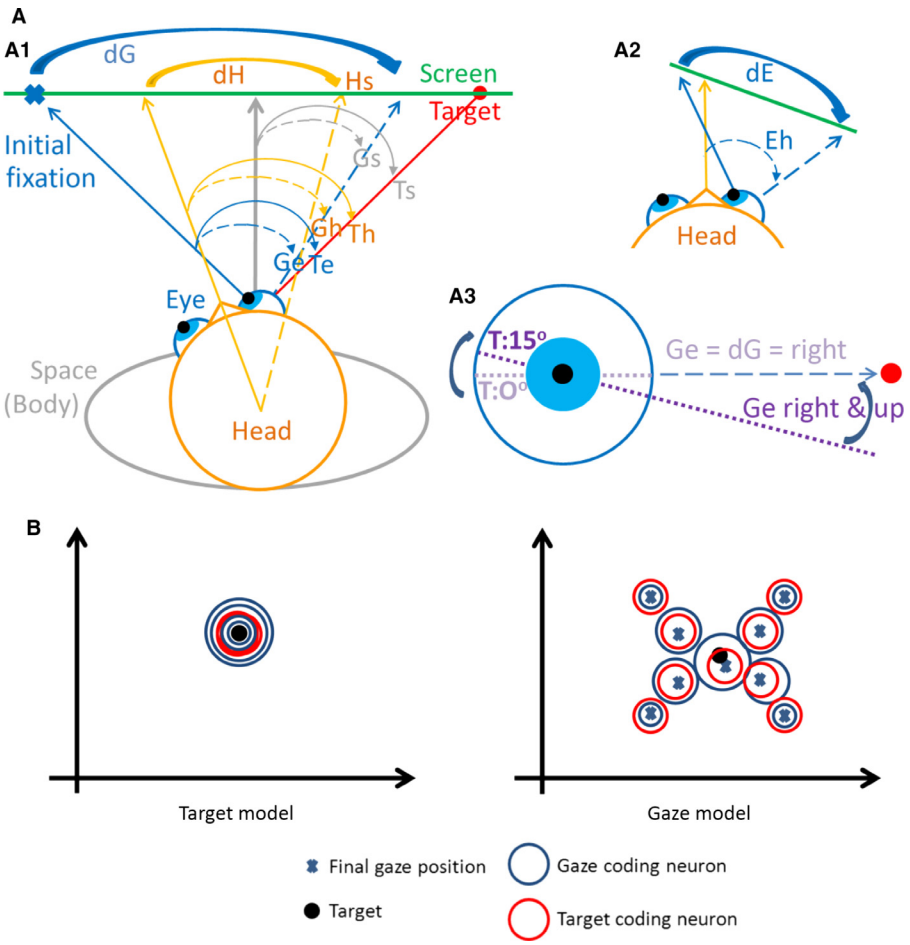

FIG. 5. (A) Geometrical interpretation of the models being tested. (A1) Most models illustrated from a view above a cartoon subject. This hypothetical example shows the space-fixed body (grey ellipse), with the head (orange ellipse) and eyes (blue circles) turned to the left towards an initial fixation point (blue cross) on the screen (green line). The solid red line and circle indicate the direction of the target on the right side of the screen. Solid blue, orange and grey arrows pointing towards the screen show initial pointing directions of gaze from the recorded eye, head, and body (fixed at midline), respectively. Dashed orange and blue lines pointing towards the screen show the final pointing direction of the head and gaze, respectively, after a future gaze shift. The heavy arrows show displacement of gaze (dG) and head (dH) pointing directions on the screen. The solid grey, orange and blue arrows curving to the right show the angular position of the target relative to space (Ts), initial head orientation (Th), and initial eye orientation (Te), respectively. The dashed gray, orange and blue arrows curving to the right show the angular position of final gaze relative to space (Gs), initial head orientation (Gh), and initial eye orientation (Ge), respectively. Final head position relative to space (Hs) is shown by the straight dashed orange arrow. (A2) Further illustration of the eye-in-head displacement model (dE; rightward curving arrow) and the eye-in-head position model (Eh; dashed blue arrow). (A3) View of the eye in space from behind, illustrating one difference between the gaze displacement (dG) model and the gaze relative to eye (Ge) model. If a target (red disc) appears to the right of the eye at the primary position, both models are equal (to the right). However, if the eye rotates torsionally (here, 15° clockwise), dG remains the same, but Ge now has an upward component. All of these parameters were allowed to vary freely in our experiment, except that initial gaze and head orientations were kept in a more central zone (see Fig. 2). Actual distances of the eyes from the screen are greater than depicted here, so translational motion of the eyes is negligible and does not affect our analysis, which was based on trial-to-trial variability of angular body positions. (B) Schematic diagram of tuning of two different neurons for two different spatial location gaze end points vs. target location. The firing rate is proportional to diameter of circles for both the target-coding neuron (○) and the gaze-coding neuron (◎). The figure on the left shows the firing rate of these two neurons for a given target location (●); the target-coding neuron fires consistently at a high rate; however, the gaze-coding neuron fires at different rates for each trial. Thus, the firing rate of the target-coding neuron is more 'coherent' in this example. The figure on the right shows that the firing rate for the gaze-coding neuron increases systematically for the preferred gaze end point location (X at the centre), whereas the firing rate of the target-coding neuron does not change with different gaze locations.

models as derived from our behavioural data for that trial. Contour fits were made to neural activity plotted as a function of the vertical and horizontal axes defined by each of these models, by use of a non-parametric method based on a series of Gaussian kernels ranging between 2° and 15° in steps of one (Keith *et al.*, 2009). This method is robust for fitting various oddly shaped or discontinuous RFs, and thus avoids the problems inherent in fitting a simple Gaussian shape to RFs that do not have a Gaussian shape (Platt & Glimcher, 1998). The model (and bandwidth) that yielded the minimum mean PRESS residuals was identified as the 'best fit' model, and was statistically compared with all other models at the same bandwidth. Specifically, a two-tailed Brown–Forsythe test was used to compare the PRESS residuals of the 'best fit' model with those of each of the other models. The model that resulted in significantly greater PRESS residuals was excluded. The analysis also accounted for the presence of any 'gain fields' (i.e. gaze position-dependent modulation) effects, but we found no significant gain field effects here, perhaps because of limitations in the range of initial gaze position. Note that the mean PRESS residuals were never reduced to zero for any model, probably because of non-spatial factors that were not accounted for in our models, such as attention, motivation, and/or random biological noise. The last step in our analysis

involved combining the results of individual neurons in order to provide an overall measure of the best model fit for population of visual and motor activities (Keith *et al.*, 2009).

Because of the predominance of Te and eye-centred gaze codes (i.e. dG and Ge) in our results (Figs 6 and 8), we constructed a continuum between Ge and Te models to test 'intermediate' Te–Ge models. This involved the calculation of PRESS residuals for models along 10 steps between and 10 steps beyond each side of these two models, and identification of the overall best fit (Sajad *et al.*, 2014). We selected Ge over dG, because it is in the same reference frame as Te, and, as a result, the constructed continuum would provide physical locations between target and gaze positions relative to the same reference frame (fixed on the eye). Te and Ge models were positioned at −5 and 5 on the continuum in each trial. The spatial models beyond Te and Ge (from −5 to −15, and from +5 to +15) were constructed to prevent false clustering at the two canonical representations. Theoretical and experimental studies have shown that individual neurons can show fits that go beyond the intermediate range between two models, that is further away from Ge than Te, or further away from Te than Ge (Pouget & Snyder, 2000; Blohm *et al.*, 2009; Patel *et al.*, 2014).

Finally, note that our analysis does not account for other factors that might modulate SC activity, such as eye velocity (Munoz *et al.*, 1991a,b; Goossens & Van Opstal, 2012), motivation levels (Isoda & Hikosaka, 2008), attention levels (Goldberg & Wurtz, 1972a,b; Shen *et al.*, 2003), plans for future gaze shifts or head movements (Monteon *et al.*, 2012), influences of eye position that do not reach statistical significance in our programme (Van Opstal *et al.*, 1995; DeSouza *et al.*, 2011), or completely random biological noise. For this reason, none of our spatial models can be expected to reduce the residuals of fit to zero for any neuron; we can only determine the best spatial fit.

Results

Neuron population

We recorded from 78 neurons from the left and right SC of two monkeys, and 60 of these neurons met our inclusion criteria (see Materials and methods). These neurons showed both 'closed' RFs (with boundaries defined within the range that we tested) and 'open' RFs (with boundaries that extended beyond the range where stimuli could be presented) with peaks varying from 4° to 30° from the fovea (see Figs 7, 9–11 for examples). On the basis of the criteria described above, 17 of these neurons were classified as visual neurons, 12 were classified as motor neurons, and 31 were classified as visuomotor neurons.

Figure 4 summarizes the average (± SEM) spike density profile for all neurons, derived either from all trials (black/grey lines) or from the neural response for trials with the top 10% number of spikes (measured in the specific time epoch explained above) (red/pink lines). The latter corresponds to trials towards the RF 'hot spot' in the preferred representation of the RF. These spike density profiles are aligned either with stimulus (Fig. 4B and C) or movement onset (Fig. 4D and E). The plots show the mean and variability of both the amplitudes and durations of our visual and motor responses (see Materials and methods). They also show the fixed temporal windows used to analyse the visual and motor responses. As noted in Materials and methods, we also used a variable motor window for the motor burst duration of each individual neuron, which varied across neurons from −100 ms to +160 ms with respect to gaze onset. Both methods produced very

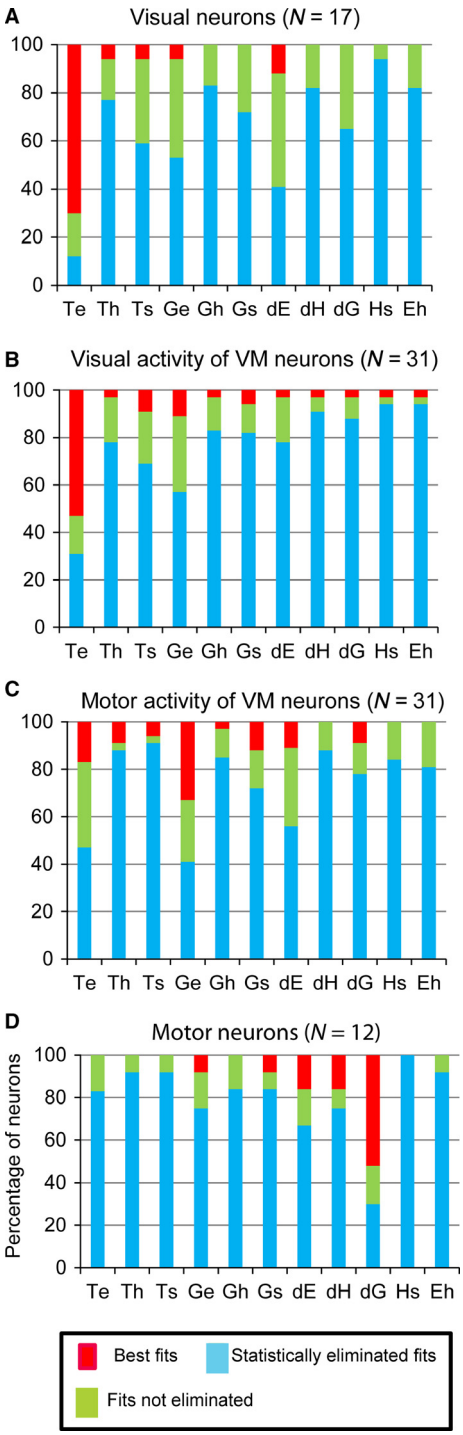

FIG. 6. Frequency histograms of goodness of fit for each model across neurons in each cell type. Best models (red) are defined as the models with the lowest residuals. The possible models (green) did not yield the lowest residual, but the residual of their fit is not significantly larger than the best fit, and thus cannot be eliminated. The worst models (blue) are the models with residuals significantly larger than those of the best model, and were thus significantly eliminated as a spatial coding possibility. (A) Distribution of results for the visual neuron population; > 60% of neurons have Te as their preferred spatial code. (B) Distribution for visual activity of visuomotor neurons, showing that the majority of neurons still prefer Te; however, the percentage is now 36%. (C) For the motor activity of visuomotor neurons, the percentage for best and possible fits at Te is decreased, and Ge has the highest percentage. (D) In motor neurons, dG is the dominant model along with dE and Ge, with no neuron having Te as its best model.

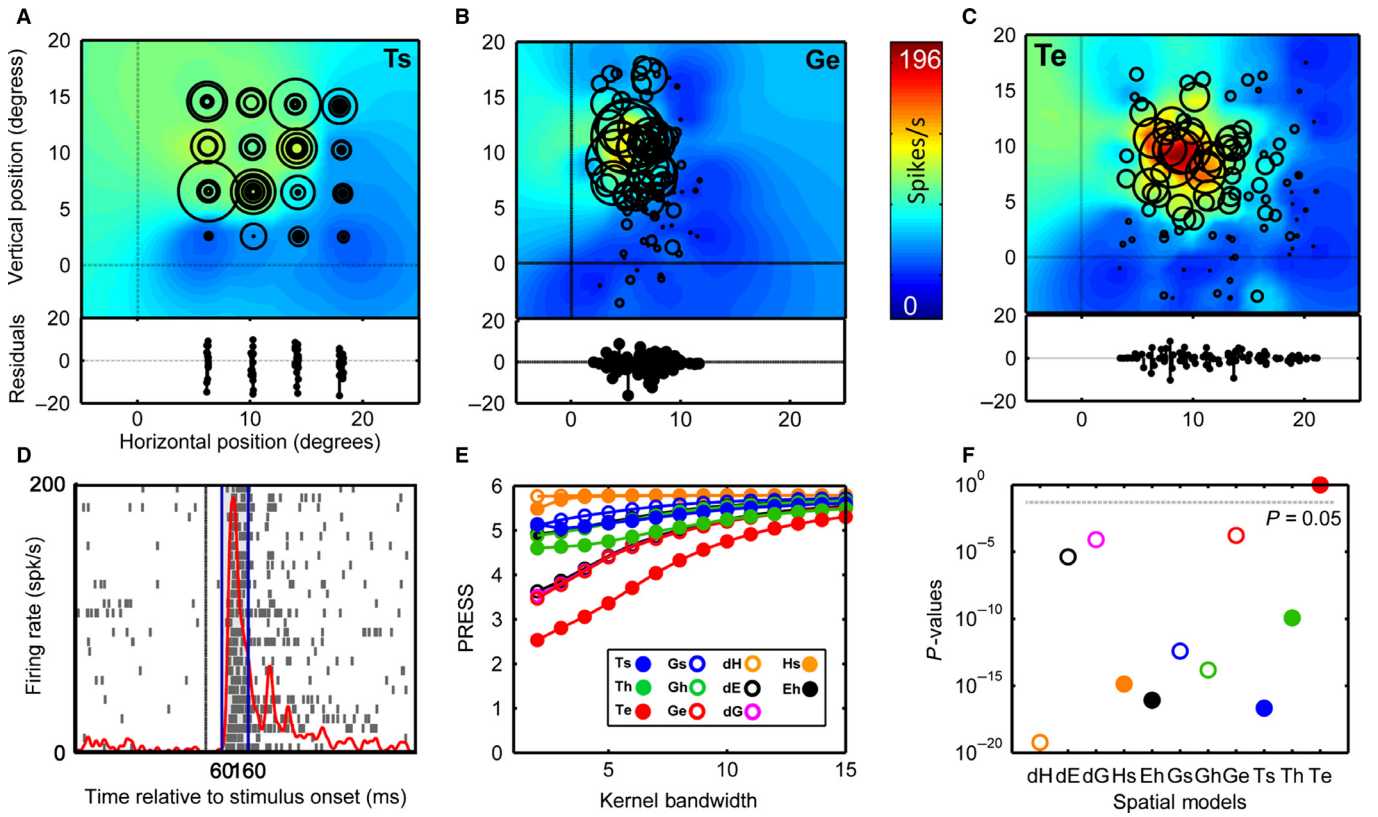

FIG. 7. Example of the analysis for a representative visual neuron. (A) RF plotted in target in space model (Ts) coordinates; the colour code represents the non-parametric fit to the model. The centres of circles represent the location of the targets in the Ts (i.e. the location of targets on the screen), and the diameter of the circles is proportional to firing rate for that given trial. The bottom panels show the residuals from fit. (B) Example of an RF plotted in final gaze relative to initial eye position models (Ge), which results in a poor-quality fit (compare the size of residuals and circle size similarities) (C) RF plotted in the target in eye model (Te), which results in a fit with significantly smaller residuals. (D) Spike density and raster plot for the top 10% firing rate of this visual neuron. The sampling window is represented by vertical blue lines; alignment is represented by vertical black line. (E) Comparison between the PRESS values of different models at the specified kernel bandwidths. (F) Statistical comparison between the best fit and other models; the dashed line represents the significant difference line, and models represented below $P = 0.05$ have significantly larger residuals and are thus eliminated as a possible spatial code.

similar results for individual neurons and at the population level (shown in Fig. 8), so, unless stated otherwise, the fixed window analysis was used to generate figures.

Note that our population motor response (and some of the individual neuron motor responses shown below) was lower than one might expect. This is likely, because: (i) we show the number of spikes of motor neurons by using the top 10% activity surrounding the peak RF response, rather than repeating saccades to the absolute peak; (ii) because head-unrestrained gaze shifts are often accompanied by longer, less intense motor bursts than head-restrained saccades (Freedman & Sparks, 1997a,b; Choi & Guitton, 2006, 2009; DeSouza *et al.*, 2011; Monteon *et al.*, 2012); and (iii) memory-guided saccades are associated with less intense motor activity than saccades made directly to a visual transient (Stanford & Sparks, 1994; DeSouza *et al.*, 2011).

The following sections examine each of these subpopulations (separately considering their visual and motor responses, as appropriate), in order to establish which candidate models of their spatial coding scheme were preferred and which could be statistically eliminated. For reference, Fig. 6 summarizes the percentage of neurons that gave a best fit (red), the percentage of neurons for which that particular model remained a possible fit (green; i.e. not statistically eliminated), and the percentage of neurons that were statistically eliminated (blue), for each of the models tested, in each frame of reference.

Visual activity

Figure 7 shows the main results of our analysis of a representative visual neuron; this includes the spike density and raster plot for the trials that have the top 10% number of spikes (Fig. 7D), RF plots for three example models (Fig. 7A–C), PRESS residuals for all models fitted with kernels of different bandwidths (Fig. 7E), and the statistical comparison between models (Fig. 7F). In the RF plots, neural activities for each trial (represented by circle size; see Fig. 5) are plotted over non-parametric model fits to these same data, indicated by the colour-coded contours. The best fit corresponds to the model and bandwidth (in this example, 2°) that gave the overall lowest residuals in Fig. 7E, and the same bandwidth was used for the other RF plots. The residuals between the data (circles) and the colour-coded fits are plotted at the bottom of Fig. 7A–C (these residuals are equivalent to the vertical difference between individual data points and a linear fit in a standard 2D regression analysis).

In order to visually illustrate the method and results for this neuron, we plotted the example neural data and their colour-coded fits relative to (i) Ts, which is roughly equivalent to target position on the screen (Fig. 7A); (ii) the model coordinates that yielded a significantly worse fit (Ge) (Fig. 7B); and (iii) the model coordinates that yielded the best fit for this neuron (Te) (Fig. 7C. This goodness of fit is explicitly indicated by the relatively small (positive or negative) residuals at the bottom of Fig. 7C as compared with Fig. 7A and Fig. 7B. The poor fit

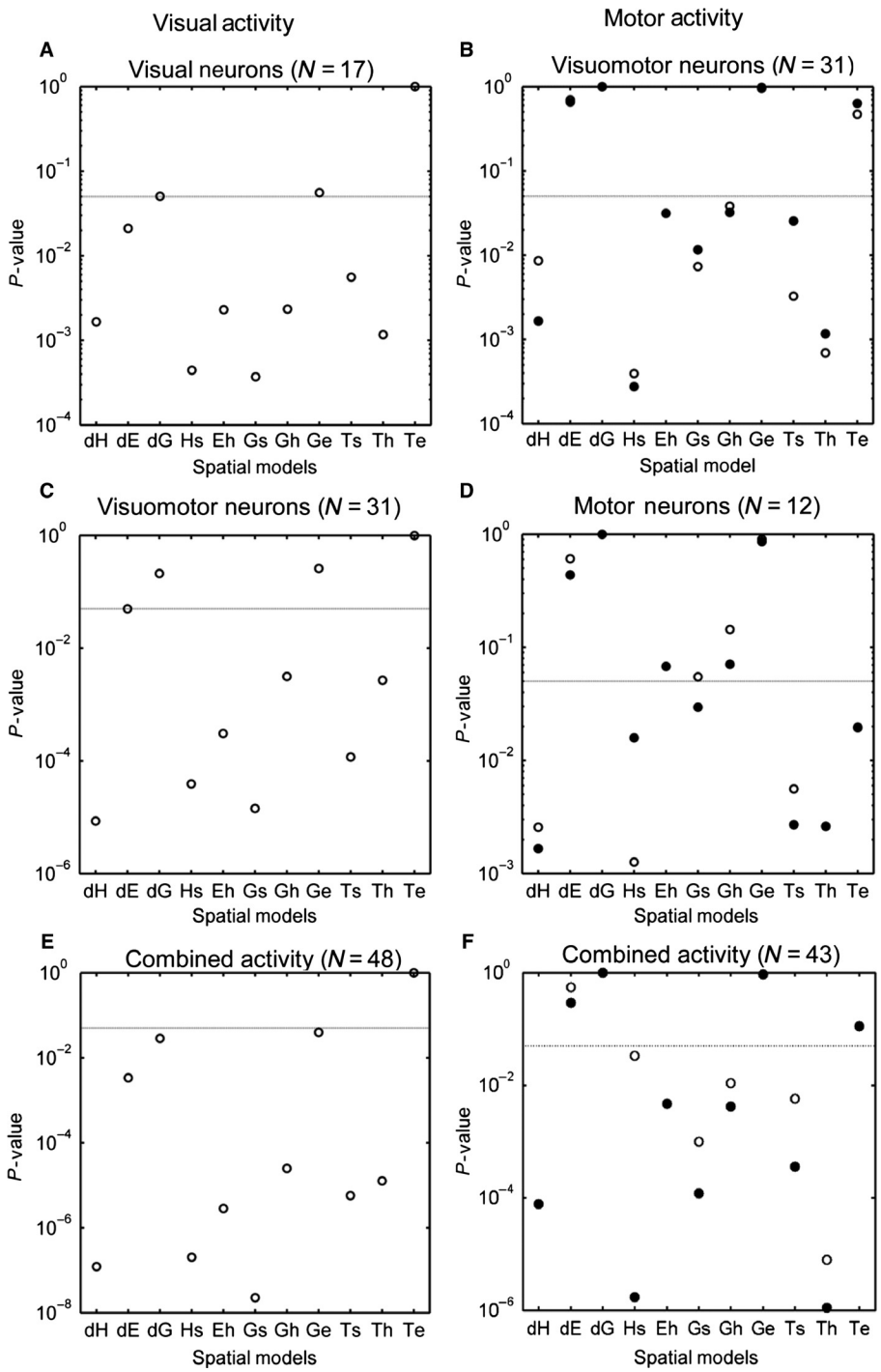

FIG. 8. Results of population analysis. (A) The visual neuron population shows a clear separation between the Te model and other models, which is represented by the horizontal line at $P = 0.05$; thus, anything below this line has a significantly larger residual and is eliminated as a possibility, and anything above this line that is not the fit with smallest residual (i.e. the best fit) is still considered as a possible spatial parameter that the activity is coding for. The results for the visual neuron population suggest that this neuron population is encoding the location of the target in eye-centred coordinates. (B) For the motor activity of visuomotor neurons, gaze-related models are better than the Te model, which suggests a change in coding within individual visuomotor neurons. (C) For the visual activity of visuomotor neurons, the best fit is still the Te model, but the separation from gaze-related models is less than for visual neurons. (D) For motor neurons, dG, as the best fit, and some other gaze-related models are among the possible coding schemes, which are, interestingly, better than the Te model, which may be attributable to another level of visuomotor transformation from visuomotor to motor neurons. For C and D, analysis was also performed with consideration of full motor burst and full duration of head movement; the results are represented by solid circles and, in cases of similar results, only solid circles are visible. (E) Population analysis for the combined activity of visual neurons and the visual component of visuomotor neurons; this indicates that the Te model is significantly preferred over all other models by the visual activity in the SC. (F) Population analysis for the combined motor activity of visuomotor neurons and of pure motor neurons; there is a trend towards coding for motor-related models, and the Te model is no longer the best fit.

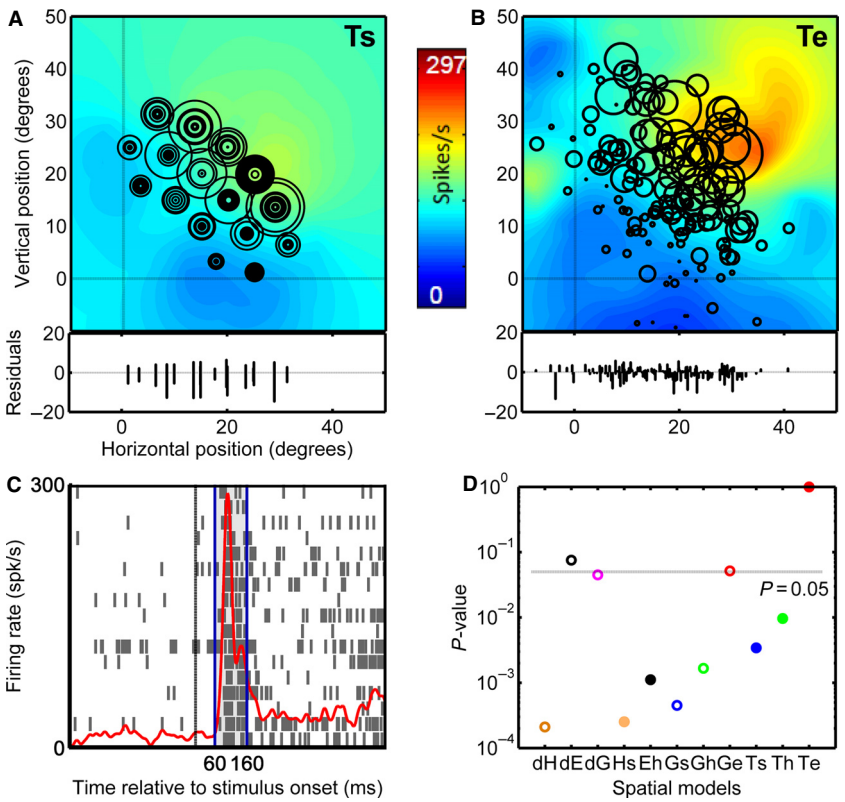

FIG. 9. An example of visual activity analysis of a representative visuomotor neuron. (A) RF plotted in the Ts model. (B) RF plotted in Te (best fit). (C) Spike density and raster plot for the visual activity. (D) Statistical comparison between the models.

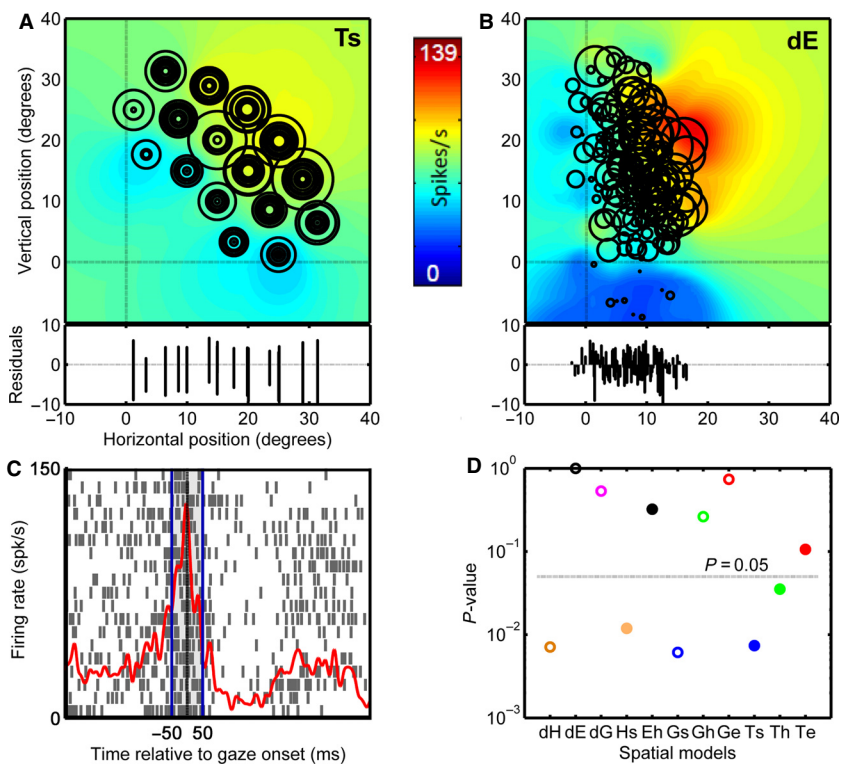

FIG. 10. An example of motor analysis for the representative visuomotor neuron shown in Fig. 9. (A) RF plotted in the Ts model. (B) RF plotted in the dE model (best fit). (C) Spike density and raster plot for the motor activity. (D) Statistical comparison between the models.

for the Ts and Ge models can also be visualized intuitively as overlap of both small and large circles (visual bursts) at the same spatial locations in Fig. 7A and B, whereas similar-sized circles cluster together in the Te model (Fig. 7C), producing a more coherent plot with larger circles in the centre and smaller circles in the periphery (as explained in Fig. 5B). This is reflected as a central hot spot in the colour-coded non-parametric fit for Te (Fig. 7C), whereas the fits appear 'washed out' in Fig. 7A and B.

The statistical analysis for this neuron is shown in Fig. 7F, which provides *P*-values comparing the residuals for the overall best model (Te fitted with a 2° bandwidth kernel) with those of every other model at that bandwidth. For this neuron, every other candidate model was statistically eliminated ($P < 0.05$). These observations held for most of our visual neurons (Fig. 6A). In 70% of these neurons, there was a significant preference for Te, with most of the remaining neurons showing a non-significant preference for Te.

It is also important to determine what information is being encoded at the population level; therefore, we combined the results of single-neuron analysis for the different populations in the study (see Materials and methods). The population analysis of visual neurons showed that the Te model was significantly better than of all the other models that we considered (Fig. 8A), except for the Ge and dG models, which were close to being statistically eliminated. These data indicate a clear preference for Te in visual neurons.

Visuomotor neurons: visual activity

Figure 9 shows an example analysis of visual activity of a representative visuomotor neuron, following similar conventions as in Fig. 6, but this time only showing: (i) the data points and colour-coded RF fit for the Ts model as a control reference (Fig. 9A); (ii) the data points and colour fit for the best RF model (Fig. 9B); (iii) the spike density and raster plot for the neuron's top 10% 'hot spot' (Fig. 9C); and (iv) statistical comparisons with the best model (Fig. 9D). In this neuron, Te still gave the best fit, but now the Ge and dE models were not significantly excluded (Fig. 9D). Across all visuomotor neurons (Fig. 6B), the visual response showed a preference for Te in most cases, and in 53% this preference was significant. At the visuomotor population level (Fig. 8C), the visual response still preferred Te, but the statistical separation between the Te, Ge and dG models showed less clear preference for the Te model than the visual response of purely visual neurons.

Visuomotor neurons: motor activity

Figure 10 shows the main results of analysis of the motor activity of the same visuomotor neuron shown in Fig. 9. Once again, we have illustrated the fit for the Ts model for reference (Fig. 10A), for the best fit model (Fig. 10B), the spike raster and density plot for the neuron (Fig. 10C), and the key statistics in Fig. 9 (Fig. 10D). In contrast to the visual activity described above, where Te was clearly preferred, the motor burst showed a general preference for (but did not clearly discriminate between) several eye and gaze models (dE, dG, Eh, Gh, and Ge) over Te, although the latter was not statistically eliminated. In other words, errors in final gaze position were reflected in variations in motor-related number of spikes in these neurons, yielding a better overall fit than target position alone. Across all individual visuomotor neurons (Fig. 6C), Ge was statistically preferred in most neurons (58%), but, overall, the preference for motor burst was more distributed among models than the visual burst described above, with no clear statistically significant 'winner'.

For the population of motor activity in visuomotor neurons (Fig. 8B), Ge produced the lowest residuals, but Te, dE and dG were very similar and were not significantly eliminated. This held for both the fixed window/head contribution to gaze analysis and the full burst/full head movement analysis. This suggests a shift in coding tendencies between the visual and motor components of visuomotor neuron activity (Fig. 8B and C), which we will quantify more directly in a subsequent section.

Motor neurons

Figure 11 summarizes the results of our analysis of a representative motor neuron with the same conventions as in Figs 9 and 10. In some respects, this neuron showed similar results to the visuomotor example shown above: the dE model and several eye-related and gaze-related models (dG, Ge, and Gs) were preferred, without a clear distinction between them. However, this time, unlike any neuron that we have shown so far, the Te model was statistically eliminated as compared with the gaze-related models. In other words, in motor neurons, fits that accounted for errors in final gaze position produced significantly lower residuals than fits that only accounted for the target location. This was the case in ~80% of the motor neurons tested (Fig. 6D). Across all neurons, dG showed the best fit in most cases, and, in some cases, this was statistically significant (Fig. 6D). However, in the population analysis (Fig. 8D), Ge and dG (which are geometrically very similar models) were nearly indistinguishable, as were several other eye and gaze models. However, importantly, Te was now significantly eliminated, for the first time, at the population level. This trend did not change when we considered full burst and duration of head movement as compared with fixed window analysis.

When the motor activity was combined into one population (Fig. 8F), the dG and Ge models gave the best fits (and were nearly identical), along with dE and Te as candidate models. Again, since the analysis considering the full burst and the full duration of head movement did not result in change to either the trend or significant separation (Fig. 8F). Our statistical analysis should work best with the largest possible range of data, including small to large movements, so the preceding analysis should not be influenced by the fact that many of our recorded head movements were small. To verify this, we repeated our full motor population analysis twice, excluding trials in which head movements were < 2° or 5°, respectively. For the > 2° head movement analysis (which eliminated 52% of our trials), Ge gave still the best overall fit. The overall pattern of results between models (not shown) was similar to that shown in Fig. 8F, except that, in this case, only Hs, Ts and Th were statistically excluded. For the > 5° head movement analysis (which eliminated 75% of our trials), Ge was still the best fit overall, and the overall pattern was again similar to that in Fig. 8F, but this time only Ts was significantly excluded. Thus, as expected, removing small head movements did not change the overall preference of the model, but simply reduced the statistical power of our analysis.

Summary and combined population analysis

To summarize the main results so far, the preferred models for all populations were gaze-centred models, but we have seen a clear transition from Te being preferred in the visual burst (Fig. 8A and C) to gaze models being slightly preferred in the motor burst of visuomotor neurons (Fig. 8B) to Te being entirely eliminated in the motor-only population (Fig. 8D). To highlight the main visuomotor trends, we also performed an analysis of the combined visual popu-

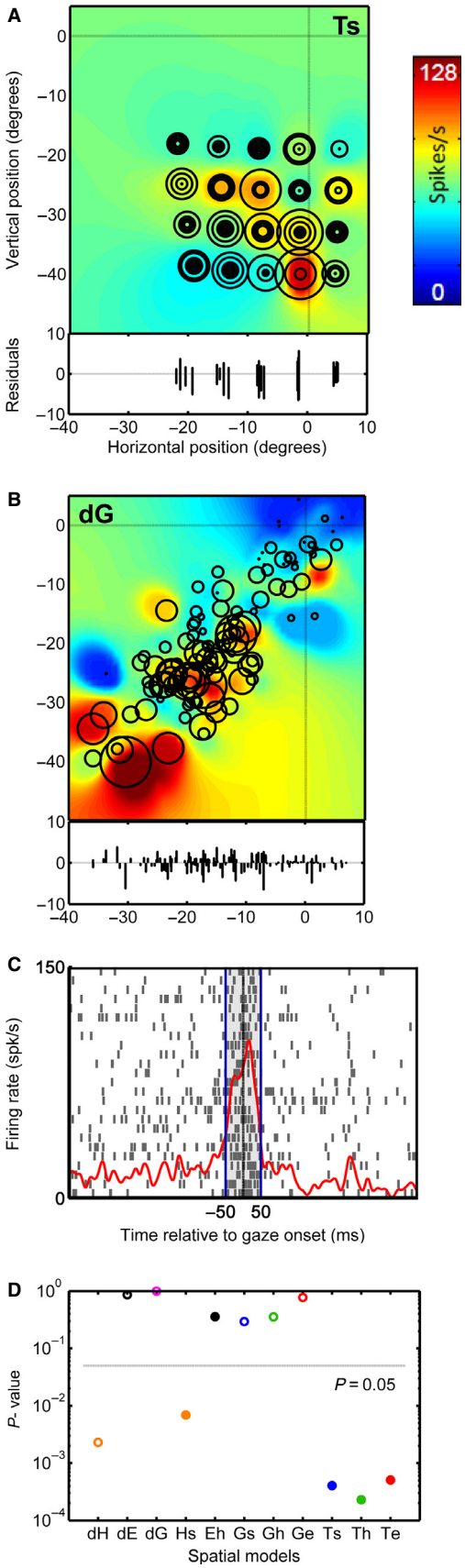

FIG. 11. An example of analysis for a representative motor neuron. (A) RF plotted in the Ts model. (B) RF plotted in the dG model (best fit). (C) Spike density and raster plot. (D) Statistical comparison between the models.

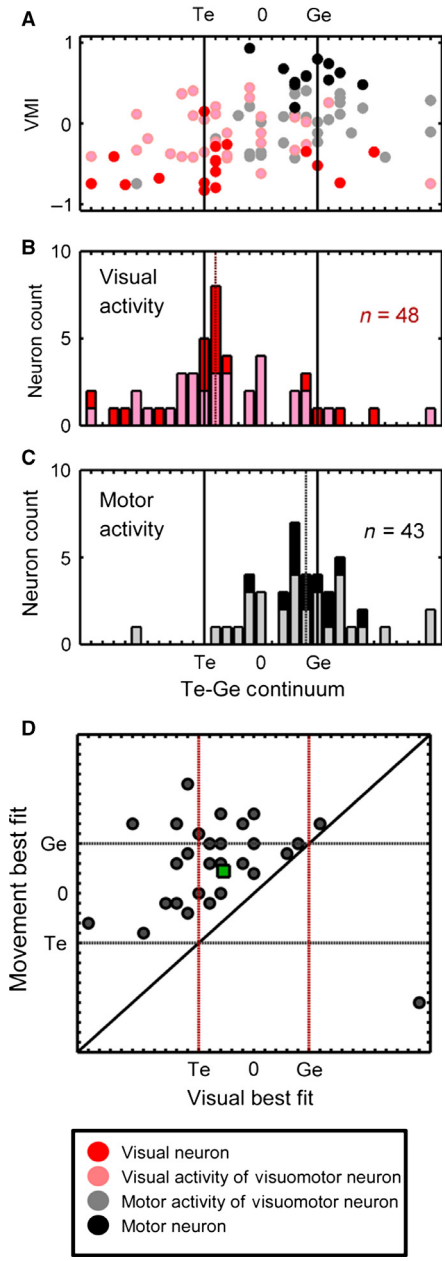

FIG. 12. Population analysis of visuomotor coding along the target–gaze continuum passing through and between the Te model and the Ge model (see Materials and methods for detailed definition). (A) Plot of VMI value for each neuron plotted as a function of its fit on the target–gaze continuum yields a weak correlation (R^2 = 0.092). (B) Frequency distribution of target vs. gaze coding of visual activity of visual neurons (red) and visuomotor neurons (pink). Note the clustering of neurons around the Te model, with a comparably low frequency of neurons represented at the gaze end of the continuum. The average target vs. gaze tendency of the population is represented by the dashed vertical red line. (C) Frequency distribution of target vs. gaze coding for motor activity of visuomotor (grey) and motor (black) neurons. Note the clustering of neurons around the Ge model, with very few representations around Te. The overall average of target vs. gaze coding of the population is represented by the vertical dashed grey line. These changes in distribution pattern between visual and motor activity and different neuronal classes further suggest a visuomotor transformation between different neuron types in the SC. (D) The target and gaze preference of visual and motor activity of visuomotor neurons. Each neuron is represented by a black circle, and the average of the population is represented by the green square. Almost all circles lie above the equality line, which is suggestive of a target–gaze-related transformation from visual to motor activity of individual visuomotor neurons.

lations and combined motor populations (Fig. 8E and F). When the visual responses from both the visual population and the visuomotor population were combined (Fig. 8E), the resulting population ($n = 48$) showed a statistical preference for the Te model over all of the other models that were considered. In the combined motor population ($n = 43$; Fig. 8F), the similar dG and Ge models were front-runners (see Discussion), with the also similar dE model lagging not far behind, followed by the Te model; all other models were statistically eliminated. We retested the full dataset after removing trials in which the head contribution to gaze was < 2°. This analysis (not shown in the figures) produced nearly identical results.

Target–gaze continuum analysis

To focus on the changes in spatial coding between our visual and motor responses, we developed a new continuum analysis between Te and Ge models. We used Ge here to represent the motor code, because it uses the same mathematical frame as Te (but note again that Ge gives nearly identical results to the geometrically similar dG).

First, we considered how the placement of a neuron along this continuum related to the relative vigour of visual vs. motor bursts, by calculating a visuomotor index (VMI) [motor spike count – visual spike count/(motor spike count + visual spike count)]. The visual and motor burst spike counts were first subtracted from the baseline activity (100-ms pre-target period). This gave a score whereby −1 is a purely visual neuron and +1 is a purely motor neuron). Neurons classified as visual had VMI values ranging from −0.83 to −0.15, visuomotor neurons had VMI values ranging from −0.74 to 0.44, and pure motor neurons had VMI values ranging from 0.2 to 0.94. Figure 12A shows the VMI plotted as a function of the Te–Ge spatial coding continuum for all neurons, and each subpopulation is colour-coded (red, visual neurons; light red, visual activity of visuomotor neurons; grey, motor activity of visuomotor neurons; and black, pure motor neurons). This leads to a very weak positive correlation ($R^2 = 0.1$ for motor response and $R^2 = 0.01$ for visual response), but one can see a general tendency for the visual responses to cluster in the lower left, and motor neurons (especially pure motor neurons) to cluster in the upper right.

Figure 12B and C (with the same horizontal axis and colour code as Fig. 12A) highlights these trends by providing frequency histograms for our different responses and neuron populations along the Te–Ge continuum. This produced a wide distribution of fits, even beyond Te and beyond Ge. This is consistent with the theory that behaviour is determined by the overall balance between members of the neuronal population, rather than individual neurons (Pouget & Snyder, 2000; Blohm *et al.*, 2009). However, within this distribution, both types of visual response (i.e. by visual and visuomotor neurons) showed their major cluster around Te (Fig. 12B), whereas both types of motor response (i.e. by visuomotor and motor neurons) showed their major cluster around Ge (Fig. 12C). In other words, along the physical continuum between target position and gaze end points, visual responses tended to encode positions near to the target, and motor responses tended to encode positions near the gaze end point. Plotted in this way showed a clear and significant shift between the coding of the visual and motor responses ($P < 0.0001$, unpaired *t*-test).

To examine whether this shift in spatial coding could occur within individual visuomotor neurons (which, by definition, show both a visual burst and a motor burst), we plotted the target–gaze continuum value of the visual vs. motor response for each visuomotor neuron (Fig. 12D). Almost all of the individual visuomotor neurons lie above the line of equality, suggesting a shift from target to gaze within these neurons. Moreover, this shift was statistically significant ($P < 0.001$, paired *t*-test) at the level of the entire visuomotor population.

Discussion

The primary goal of this study was to determine what spatial information is encoded within temporally defined visual and motor responses in the primate SC during head-unrestrained gaze shifts. Our analysis allowed us to simultaneously compare all of the potential candidate models that have been considered in the literature. The results showed a statistical preference for eye-centred coding of target position in the visual response vs. final gaze position coding in the motor response, even within visuomotor cells. Furthermore, a more subtle trend emerged across neuron subpopulations, with target coding being most prominent in the vision-only cells, being progressively less so in the visual and motor responses of visuomotor cells, and finally being statistically eliminated in pure motor cells. In contrast, we found no clear evidence for effector-specific coding or non-retinal frames of reference in our behavioural paradigm.

Visuomotor transformation

Although the SC is closely associated with visuomotor transformations (Schiller & Wurtz, 1975; Sparks, 1986, 1988; Gandhi & Katnani, 2011; Katnani & Gandhi, 2011), it remained unclear to what degree these transformations occur within the SC (Takeichi *et al.*, 2007) as opposed to downstream from the SC (Klier *et al.*, 2001, 2003a,b; Edelman & Goldberg, 2002). In anti-saccade experiments, visual responses are tied to the location of the visual stimulus, whereas motor responses are linked to the direction of the saccade (Everling *et al.*, 1999a,b; Edelman & Goldberg, 2001). However, in anti-saccade experiments, animals might imagine a target opposite to the stimulus (Zhang & Barash, 2000; Munoz & Everling, 2004; Fernandez-Ruiz *et al.*, 2007). Consistent with this, SC activity correlates better with target position than position-dependent errors in memory-guided saccades (Sparks, 1989; Gnadt *et al.*, 1991; Stanford & Sparks, 1994; Edelman & Goldberg, 2001). Furthermore, when targets and saccades are dissociated through weakening of the eye muscles or visual feedback training, SC activity is also linked to target location (Frens & Van Opstal, 1997; Edelman & Goldberg, 2002; Quessy *et al.*, 2010), although one study suggested that SC activity can reflect saccadic adaptation (Takeichi *et al.*, 2007). These results are important, but it is not trivial to extrapolate from a perturbed system to the normal system, especially if the adaptation mechanism (e.g. the cerebellum) operates in parallel with the main sensorimotor channel (Optican & Robinson, 1980; Quaia *et al.*, 1999; Straube *et al.*, 2001).

One advantage of our approach is that the visuomotor separation was accomplished simply through natural, untrained variability in gaze end points (Platt & Glimcher, 1998). Previously, when we applied this method to a pooled visual and motor response across all types of SC neurons in a visually guided gaze task (i.e. no delay to separate visual and motor activity types), target coding dominated the results (DeSouza *et al.*, 2011). If we pooled all of the data in the current study, we would probably obtain the same results, as the Te model is so dominant in visual responses and remains a candidate model for motor responses in visuomotor neurons. However, when we separated the 'visual response' from the 'motor response',

we found that: (i) pure visual neurons encode the location of the target; (ii) target coding is also preferred, but less distinctly, in the visual response of visuomotor neurons; (ii) the motor response of visuomotor neurons preferentially encodes final gaze position; and (iv) this preference becomes most distinct in pure motor cells, where target coding is statistically eliminated. On the basis of these findings, it is tempting to posit a progressive transformation between the sensory signal in visual neurons to a behavioral output in the pure motor neurons.

If this is true, it does not mean that these transformations are occurring exclusively within and between SC neurons. Although some SC visual cells are known to receive direct input from the retina (Sparks, 1986), and SC motor responses directly influence reticular formation saccade responses (Yasui *et al.*, 1994; Rodgers *et al.*, 2006), the intermediate connections between the superficial and deep layers of the SC involve complex pathways involving the cerebral cortex (Wurtz & Albano, 1980), and the SC receives feedback from the brainstem burst generator (Moschovakis *et al.*, 1988). Thus, this signal progression could reflect events throughout the entire saccade system. Consistent with this, in a recent study of frontal eye field activity using very similar methods, we found a similar transition from visual to motor coding (Sajad *et al.*, 2014). However, in our SC data, the visuomotor progression was more complete at the level of pure motor neurons.

Another limitation of our study is that we did not establish which of our cells project to the brainstem gaze control generator vs. feedback to the thalamus/cortex (Wurtz & Sommer 2004). However, these schemes do not conflict, because visuomotor and motor cells tend to provide such projections (Sommer & Wurtz 2000, Wurtz *et al.* 2001), and our results suggest that these cells would provide the most accurate estimate of actual gaze motion.

No previous study has compared the visual activity of these various SC neuron types in terms of target vs. gaze parameter codes. Some studies have proposed that distinct subgroups of visuomotor neuron populations are involved in transferring the retinal error signal of the visual activity to downstream structures, for example the quasivisual cells (Mays & Sparks, 1980) and the visually triggered movement cells (Mohler & Wurtz, 1976), but these studies did not suggest a transformation in spatial information until further downstream (Sparks, 1986, 1988, 2002; Hepp *et al.*, 1993; Stanford & Sparks, 1994). The current study suggests that the SC does not simply relay the retinal code; it is also involved in a transformation.

One of our most striking findings was the significant shift of coding along the target–gaze continuum between the visual and motor bursts of visuomotor cells, with this trend being clear within almost all individual neurons. This has never been shown before in SC visuomotor cells in 'pro' saccades, but similar observations have been made with other saccade and reach paradigms in the dorsal premotor cortex (Caminiti *et al.*, 1991; Crammond & Kalaska, 2000), the primary motor cortex (Ashe & Georgopoulos, 1994), the posterior parietal cortex (Buneo *et al.*, 2002; Bremner & Andersen, 2012), the prefrontal cortex (Funahashi *et al.*, 1990), the frontal eye field (Everling & Munoz, 2000; Sajad *et al.*, 2014), and the lateral intraparietal cortex (Barash *et al.*, 1991a,b).

How and when does this transformation arise? In our memory-delay paradigm, it is possible that the visuomotor transformation occurs between visual and delay responses, during the delay, or in the transformation from delay activity to motor activity. This evokes the possibility that the gaze signal 'wanders away' from the target signal owing to faulty recurrent feedback in the short-term memory circuit (Compte *et al.*, 2000; Chang *et al.*, 2012; Sajad *et al.*, 2014; Wimmer *et al.*, 2014). Another possibility is that the differences between visual and motor codes arise at the time of the motor burst, owing to feedback signals that are not present in the visual response (Soetedjo *et al.*, 2002; Matsuo *et al.*, 2004; Choi & Guitton, 2006, 2009). For example, some models and evidence suggest that, during gaze shifts, SC motor responses are influenced by a brainstem feedback loop that would tend to relay highly accurate measures of the actual metrics of the gaze shift (Robinson, 1973; Becker & Jürgens, 1979; Everling *et al.*, 1998; Guitton *et al.*, 2003).

Effector specificity

A crucial aspect of gaze control is the decomposition of target position into separate commands for gaze (or the eye) vs. the head (Daye *et al.*, 2014). Unlike our previous study (DeSouza *et al.*, 2011), here we were able to distinguish whether the motor activity of SC neurons is coding for movement vectors, or final positions of eye or head, as opposed to gaze models (dE, dH, Eh, and Hs, respectively) as opposed to gaze models. Consistent with our frontal eye field results (Sajad *et al.*, 2014), we found that, overall, SC motor activity fits best with gaze-related models (Ge and dG), although the eye displacement model (dE) was not significantly eliminated. This was probably because eye displacement dominated the gaze shifts in our animals, so dE was very similar to the gaze displacement models. However, the dH model was significantly eliminated in all of our motor activity populations, even when we considered the full burst and head movement durations. This agrees with most previous studies, which have suggested that the saccade-related activity in the SC is better correlated with gaze motion than with eye motion, and is only poorly related to head movements alone (Freedman & Sparks, 1997b). It has been suggested that 2D gaze displacement signals from the SC are dissociated downstream by the brainstem into separate 3D eye and head control signals (Klier *et al.*, 2003a,b; Stuphorn, 2007; Kremmyda *et al.*, 2011), probably involving signals from the cerebellum and vestibular system (Van Opstal *et al.*, 1996; Straumann *et al.*, 2000; Glasauer *et al.*, 2003; Lehnen *et al.*, 2008).

This seems to contradict some studies that have found head-related activity in the SC (Walton *et al.*, 2007; Gandhi & Katnani, 2011; Monteon *et al.*, 2012). However, some of these recordings may have involved a different class of cells than that described here (Walton *et al.*, 2007). Moreover, it should be noted that our method only describes which parameter best describes the organization of visual and motor RFs, and we only mapped these RFs from relatively central gaze/head positions. It is possible that weaker signals were present but were still statistically eliminated by our method. For example, when we plotted model fits against motor activity along the continuum between gaze displacement and head displacement models (not shown here), there was a slight shift in the overall average away from gaze towards the head, probably because a few motor neurons did prefer the head displacement model (Fig. 6D). Furthermore, our finding does not eliminate the possible contribution of other parameters, including head position and motion, in other aspects of gaze control. For example, large head position and movement modulations have been observed in the SC in experiments that deliberately dissociated eye and head displacement and/or used very large excursions in head position. These responses may reflect other aspects of SC organization (Gandhi & Katnani, 2011; Monteon *et al.*, 2012; Daye *et al.*, 2014). Thus, to be conservative, our current results should only be interpreted in the context of centre-out movements and their contri-

bution to the spatial organization of visual and motor receptive fields in the SC.

Frames of reference

For a successful visuomotor transformation, the frame of reference of sensory input (here, the eye) has to ultimately be transferred into an appropriate frame for muscle contraction (here, eye rotation relative to head and head rotation relative to the torso). The areas of the brain involved in sensorimotor transformations contain a complex array of signals, with some areas showing intermediate frames of reference (Avillac *et al.*, 2005; Mullette-Gillman *et al.*, 2005, 2009; Monteon *et al.*, 2013). Nevertheless, eye-centred representations often dominate the early stages of visuomotor transformations (Buneo *et al.*, 2002; Crawford *et al.*, 2011). This is consistent with most head-fixed studies (Andersen *et al.*, 1985; Sparks, 1989; Chen *et al.*, 1993; Cohen & Andersen, 2002), and extends to head-unrestrained studies of the SC (Klier *et al.*, 2001; DeSouza *et al.*, 2011).

In the current SC study – much as in our recent frontal eye field study (Sajad *et al.*, 2014) – gaze-centred representations again predominated; that is, Te and Ge were the two most common best fits across all visual and motor responses, followed by dG. Te clearly dominated the visual response, but we could not separate the Ge (final gaze position relative to eye) and dG (gaze displacement, which is the same as the projection of final gaze position relative to the fixation point on screen) models in our motor responses. Both are gaze-centred, in the sense that initial gaze direction is the '0' in this coordinate system, but the coordinate axes for dG are actually fixed in space, whereas the coordinate axes of Ge are fixed in the eye (Crawford & Guitton, 1997). This necessitates a 3D position transformation between Ge and dG (Blohm & Lefèvre, 2010). Our data suggest that such a transformation could occur between visuomotor neurons (which fit Ge best) and motor neurons (which fit dG best), but, unfortunately, the population analyses for these models gave results that were nearly identical and certainly not statistically different. This is probably because these two models are geometrically very similar up to gaze excursions of 30° (Fig. 3), which encompasses most of the data recorded here (Crawford & Guitton, 1997). Furthermore, our larger gaze shifts (30–50°) tended to fall beyond the range of RFs sensitive to our statistical method: either because they went beyond the region of activity in a closed receptive field, or because they reached the plateau area of an open receptive field, where there was little directional modulation. On the basis of this RF organization, it is not obvious how humans and monkeys are able to produce accurate directional modulations in very large gaze shifts (Klier & Crawford, 1998; Klier *et al.*, 2001).

A previous stimulation study was able to separate these models by evoking very large gaze shifts from the posterior SC, and here, the Ge model was clearly preferred (Klier *et al.*, 2001). Thus, the most parsimonious explanation for our results is that the motor output of the SC encodes Ge, but it is possible that the SC is able to transform Te signals (from visual input or from electrical stimulation) into a dG output in its motor response as a function of intrinsic gaze position signals (Van Opstal *et al.*, 1995; Smith & Crawford, 2005; DeSouza *et al.*, 2011). Testing between these options will require further experiments that focus on very large gaze shifts and/or gaze shifts from large torsional offsets in eye positions. Furthermore, this would require either the localization of closed receptive fields with peaks very far from the fovea (which we never observed here), or perhaps simultaneous recordings from multiple sites in the SC, to understand how the precise direction of large gaze shifts is encoded at a population level.

Conflicts of interest

The authors declare that there are no conflicts of interest.

Acknowledgements

This project was supported by a grant from the Canadian Institutes of Health Research. J. D. Crawford is supported by a Canada Research Chair award. M. Sadeh and A. Sajad were supported by Ontario Graduate Scholarships. The authors thank S. Sun for computer programming support, and Dr G. P. Keith for his help in developing the theory and analysis software for this project.

Abbreviations

dE, vector displacement (i.e. final position minus initial position) of the eye during gaze shifts (i.e. the saccade); dG, gaze in space (i.e. gaze displacement vector as projected onto a 2D screen); Ge, final gaze position relative to initial eye orientation; Te, target location relative to initial 3D eye orientation; Ts, target location relative to in the space-fixed (or body-fixed) coordinates; VMI, visuomotor index.

References

Andersen, R.A., Essick, G.K. & Siegel, R.M. (1985) Encoding of spatial location by posterior parietal neurons. *Science*, **230**, 456–458.
Ashe, J. & Georgopoulos, A.P. (1994) Movement parameters and neural activity in motor cortex and area 5. *Cereb. Cortex*, **4**, 590–600.
Avillac, M., Deneve, S., Olivier, E., Pouget, A. & Duhamel, J.R. (2005) Reference frames for representing visual and tactile locations in parietal cortex. *Nat. Neurosci.*, **8**, 941–949.
Barash, S., Bracewell, R.M., Fogassi, L., Gnadt, J.W. & Andersen, R.A. (1991a) Saccade-related activity in the lateral intraparietal area. I. Temporal properties; comparison with area 7a. *J. Neurophysiol.*, **66**, 1095–1108.
Barash, S., Bracewell, R.M., Fogassi, L., Gnadt, J.W. & Andersen, R.A. (1991b) Saccade-related activity in the lateral intraparietal area. II. Spatial properties. *J. Neurophysiol.*, **66**, 1109–1124.
Becker, W. & Jürgens, R. (1979) An analysis of the saccadic system by means of double step stimuli. *Vision Res.*, **19**, 967–983.
Berson, D.M. (1988) Retinal and cortical inputs to cat superior colliculus: composition, convergence and laminar specificity. *Prog. Brain Res.*, **75**, 17–26.
Blohm, G. & Lefèvre, P. (2010) Visuomotor velocity transformations for smooth pursuit eye movements. *J. Neurophysiol.*, **104**, 2103–2115.
Blohm, G., Keith, G.P. & Crawford, J.D. (2009) Decoding the cortical transformations for visually guided reaching in 3D space. *Cereb. Cortex*, **19**, 1372–1393.
Bremner, L.R. & Andersen, R.A. (2012) Coding of the reach vector in parietal area 5d. *Neuron*, **75**, 342–351.
Buneo, C.A., Jarvis, M.R., Batista, A.P. & Andersen, R.A. (2002) Direct visuomotor transformations for reaching. *Nature*, **416**, 632–636.
Caminiti, R., Johnson, P.B., Galli, C., Ferraina, S. & Burnod, Y. (1991) Making arm movements within different parts of space: the premotor and motor cortical representation of a coordinate system for reaching to visual targets. *J. Neurosci.*, **11**, 1182–1197.
Chang, M.H., Armstrong, K.M. & Moore, T. (2012) Dissociation of response variability from firing rate effects in frontal eye field neurons during visual stimulation, working memory, and attention. *J. Neurosci.*, **32**, 2204–2216.
Chen, Y., Getchell, T.V., Sparks, D.L. & Getchell, M.L. (1993) Patterns of adrenergic and peptidergic innervation in human olfactory mucosa: age-related trends. *J. Comp. Neurol.*, **334**, 104–116.
Choi, W.Y. & Guitton, D. (2006) Responses of collicular fixation neurons to gaze shift perturbations in head-unrestrained monkey reveal gaze feedback control. *Neuron*, **50**, 491–505.
Choi, W.Y. & Guitton, D. (2009) Firing patterns in superior colliculus of head-unrestrained monkey during normal and perturbed gaze saccades reveal short-latency feedback and a sluggish rostral shift in activity. *J. Neurosci.*, **29**, 7166–7180.
Cohen, Y.E. & Andersen, R.A. (2002) A common reference frame for movement plans in the posterior parietal cortex. *Nat. Rev. Neurosci.*, **3**, 553–562.
Compte, A., Brunel, N., Goldman-Rakic, P.S. & Wang, X.J. (2000) Synaptic mechanisms and network dynamics underlying spatial working memory in a cortical network model. *Cereb. Cortex*, **10**, 910–923.

Cowie, R.J. & Robinson, D.L. (1994) Subcortical contributions to head movements in macaques. I. Contrasting effects of electrical stimulation of a medial pontomedullary region and the superior colliculus. *J. Neurophysiol.*, **72**, 2648–2664.

Cowie, R.J., Smith, M.K. & Robinson, D.L. (1994) Subcortical contributions to head movements in macaques. II. Connections of a medial pontomedullary head-movement region. *J. Neurophysiol.*, **72**, 2665–2682.

Crammond, D.J. & Kalaska, J.F. (2000) Prior information in motor and premotor cortex: activity during the delay period and effect on pre-movement activity. *J. Neurophysiol.*, **84**, 986–1005.

Crawford, J.D. & Guitton, D. (1997) Visual-motor transformations required for accurate and kinematically correct saccades. *J. Neurophysiol.*, **78**, 1447–1467.

Crawford, J.D., Ceylan, M.Z., Klier, E.M. & Guitton, D. (1999) Three-dimensional eye–head coordination during gaze saccades in the primate. *J. Neurophysiol.*, **81**, 1760–1782.

Crawford, J.D., Henriques, D.Y. & Medendorp, W.P. (2011) Three-dimensional transformations for goal-directed action. *Annu. Rev. Neurosci.*, **34**, 309–331.

Cynader, M. & Berman, N. (1972) Receptive-field organization of monkey superior colliculus. *J. Neurophysiol.*, **35**, 187–201.

Daye, P.M., Optican, L.M., Blohm, G. & Lefèvre, P. (2014) Hierarchical control of two-dimensional gaze saccades. *J. Comput. Neurosci.*, **36**, 355–382.

DeSouza, J.F., Keith, G.P., Yan, X., Blohm, G., Wang, H. & Crawford, J.D. (2011) Intrinsic reference frames of superior colliculus visuomotor receptive fields during head-unrestrained gaze shifts. *J. Neurosci.*, **31**, 18313–18326.

Edelman, J.A. & Goldberg, M.E. (2001) Dependence of saccade-related activity in the primate superior colliculus on visual target presence. *J. Neurophysiol.*, **86**, 676–691.

Edelman, J.A. & Goldberg, M.E. (2002) Effect of short-term saccadic adaptation on saccades evoked by electrical stimulation in the primate superior colliculus. *J. Neurophysiol.*, **87**, 1915–1923.

Everling, S. & Munoz, D.P. (2000) Neuronal correlates for preparatory set associated with pro-saccades and anti-saccades in the primate frontal eye field. *J. Neurosci.*, **20**, 387–400.

Everling, S., Paré, M., Dorris, M.C. & Munoz, D.P. (1998) Comparison of the discharge characteristics of brain stem omnipause neurons and superior colliculus fixation neurons in monkey: implications for control of fixation and saccade behavior. *J. Neurophysiol.*, **79**, 511–528.

Everling, S., Bell, A.H., Dorris, M.C., Klein, R.M. & Munoz, D.P. (1999a) Comparison of pro-and antisaccades in non-human primates: II. Neural activity in the superior colliculus and frontal eye field. *J. Cognitive Neurosci. (Suppl.)*, 92.

Everling, S., Dorris, M.C., Klein, R.M. & Munoz, D.P. (1999b) Role of primate superior colliculus in preparation and execution of anti-saccades and pro-saccades. *J. Neurosci.*, **19**, 2740–2754.

Fernandez-Ruiz, J., Goltz, H.C., DeSouza, J.F., Vilis, T. & Crawford, J.D. (2007) Human parietal 'reach region' primarily encodes intrinsic visual direction, not extrinsic movement direction, in a visual motor dissociation task. *Cereb. Cortex*, **17**, 2283–2292.

Freedman, E.G. & Sparks, D.L. (1997a) Eye–head coordination during head-unrestrained gaze shifts in rhesus monkeys. *J. Neurophysiol.*, **77**, 2328–2348.

Freedman, E.G. & Sparks, D.L. (1997b) Activity of cells in the deeper layers of the superior colliculus of the rhesus monkey: evidence for a gaze displacement command. *J. Neurophysiol.*, **78**, 1669–1690.

Frens, M.A. & Van Opstal, A.J. (1997) Monkey superior colliculus activity during short-term saccadic adaptation. *Brain Res. Bull.*, **43**, 473–483.

Funahashi, S., Bruce, C.J. & Goldman-Rakic, P.S. (1990) Visuospatial coding in primate prefrontal neurons revealed by oculomotor paradigms. *J. Neurophysiol.*, **63**, 814–831.

Gandhi, N.J. & Katnani, H.A. (2011) Motor functions of the superior colliculus. *Annu. Rev. Neurosci.*, **34**, 205–231.

Glasauer, S., Hoshi, M., Kempermann, U., Eggert, T. & Büttner, U. (2003) Three-dimensional eye position and slow phase velocity in humans with downbeat nystagmus. *J. Neurophysiol.*, **89**, 338–354.

Gnadt, J.W., Bracewell, R.M. & Andersen, R.A. (1991) Sensorimotor transformation during eye movements to remembered visual targets. *Vision Res.*, **31**, 693–715.

Goldberg, M.E. & Wurtz, R.H. (1972a) Activity of superior colliculus in behaving monkey. I. Visual receptive fields of single neurons. *J. Neurophysiol.*, **35**, 542–559.

Goldberg, M.E. & Wurtz, R.H. (1972b) Activity of superior colliculus in behaving monkey. II. Effect of attention on neuronal responses. *J. Neurophysiol.*, **35**, 560–574.

Goossens, H.H. & Van Opstal, A.J. (2012) Optimal control of saccades by spatial temporal activity patterns in the monkey superior colliculus. *PLoS Comput. Biol.*, **8**, e1002508.

Guitton, D., Crommelinck, M. & Roucoux, A. (1980) Stimulation of the superior colliculus in the alert cat. I. Eye movements and neck EMG activity evoked when the head is restrained. *Exp. Brain Res.*, **39**, 63–73.

Guitton, D., Bergeron, A., Choi, W.Y. & Matsuo, S. (2003) On the feedback control of orienting gaze shifts made with eye and head movements. *Prog. Brain Res.*, **142**, 55–68.

Hartwich-Young, R., Nelson, J.S. & Sparks, D.L. (1990) The perihypoglossal projection to the superior colliculus in the rhesus monkey. *Visual Neurosci.*, **4**, 29–42.

Hepp, K., Van Opstal, A.J., Straumann, D., Hess, B.J. & Henn, V. (1993) Monkey superior colliculus represents rapid eye movements in a two-dimensional motor map. *J. Neurophysiol.*, **69**, 965–979.

Isoda, M. & Hikosaka, O. (2008) A neural correlate of motivational conflict in the superior colliculus of the macaque. *J. Neurophysiol.*, **100**, 1332–1342.

Katnani, H.A. & Gandhi, N.J. (2011) Order of operations for decoding superior colliculus activity for saccade generation. *J. Neurophysiol.*, **106**, 1250–1259.

Keith, G.P. & Crawford, J.D. (2008) Saccade-related remapping of target representations between topographic maps: a neural network study. *J. comput. Neurosci.*, **24**, 157–178.

Keith, G.P., DeSouza, J.F., Yan, X., Wang, H. & Crawford, J.D. (2009) A method for mapping response fields and determining intrinsic reference frames of single-unit activity: applied to 3D head-unrestrained gaze shifts. *J. Neurosci. Meth.*, **180**, 171–184.

Klier, E.M. & Crawford, J.D. (1998) Human oculomotor system accounts for 3-D eye orientation in the visual-motor transformation for saccades. *J. Neurophysiol.*, **80**, 2274–2294.

Klier, E.M., Wang, H. & Crawford, J.D. (2001) The superior colliculus encodes gaze commands in retinal coordinates. *Nat. Neurosci.*, **4**, 627–632.

Klier, E.M., Martinez-Trujillo, J.C., Medendorp, W.P., Smith, M.A. & Crawford, J.D. (2003a) Neural control of 3-D gaze shifts in the primate. *Prog. Brain Res.*, **142**, 109–124.

Klier, E.M., Wang, H. & Crawford, J.D. (2003b) Three-dimensional eye-head coordination is implemented downstream from the superior colliculus. *J. Neurophysiol.*, **89**, 2839–2853.

Kremmyda, O., Glasauer, S., Guerrasio, L. & Büttner, U. (2011) Effects of unilateral midbrain lesions on gaze (eye and head) movements. *Ann. N.Y. Acad. Sci.*, **1233**, 71–77.

Lee, J. & Groh, J.M. (2012) Auditory signals evolve from hybrid- to eye-centered coordinates in the primate superior colliculus. *J. Neurophysiol.*, **108**, 227–242.

Lehnen, N., Büttner, U. & Glasauer, S. (2008) Head movement control during head-free gaze shifts. *Prog. Brain Res.*, **171**, 331–334.

Marino, R.A., Rodgers, C.K., Levy, R. & Munoz, D.P. (2008) Spatial relationships of visuomotor transformations in the superior colliculus map. *J. Neurophysiol.*, **100**, 2564–2576.

Marrocco, R.T. & Li, R.H. (1977) Monkey superior colliculus: properties of single cells and their afferent inputs. *J. Neurophysiol.*, **40**, 844–860.

Martinez-Trujillo, J.C., Klier, E.M., Wang, H. & Crawford, J.D. (2003) Contribution of head movement to gaze command coding in monkey frontal cortex and superior colliculus. *J. Neurophysiol.*, **90**, 2770–2776.

Matsuo, S., Bergeron, A. & Guitton, D. (2004) Evidence for gaze feedback to the cat superior colliculus: discharges reflect gaze trajectory perturbations. *J. Neurosci.*, **24**, 2760–2773.

Mays, L.E. & Sparks, D.L. (1980) Dissociation of visual and saccade-related responses in superior colliculus neurons. *J. Neurophysiol.*, **43**, 207–232.

McIlwain, J.T. (1986) Effects of eye position on saccades evoked electrically from superior colliculus of alert cats. *J. Neurophysiol.*, **55**, 97–112.

Mohler, C.W. & Wurtz, R.H. (1976) Organization of monkey superior colliculus: intermediate layer cells discharging before eye movements. *J. Neurophysiol.*, **39**, 722–744.

Monteon, J.A., Avillac, M., Yan, X., Wang, H. & Crawford, J.D. (2012) Neural mechanisms for predictive head movement strategies during sequential gaze shifts. *J. Neurophysiol.*, **108**, 2689–2707.

Monteon, J.A., Wang, H., Martinez-Trujillo, J. & Crawford, J.D. (2013) Frames of reference for eye-head gaze shifts evoked during frontal eye field stimulation. *Eur. J. Neurosci.*, **37**, 1754–1765.

Moschovakis, A., Karabelas, A. & Highstein, S. (1988) Structure–function relationships in the primate superior colliculus. I. Morphological classification of efferent neurons. *J. Neurophysiol.*, **60**, 232–262.

Mullette-Gillman, O.A., Cohen, Y.E. & Groh, J.M. (2005) Eye-centered, head-centered, and complex coding of visual and auditory targets in the intraparietal sulcus. *J. Neurophysiol.*, **94**, 2331–2352.
Mullette-Gillman, O.A., Cohen, Y.E. & Groh, J.M. (2009) Motor-related signals in the intraparietal cortex encode locations in a hybrid, rather than eye-centered reference frame. *Cereb. Cortex*, **19**, 1761–1775.
Munoz, D.P. & Everling, S. (2004) Look away: the anti-saccade task and the voluntary control of eye movement. *Nat. Rev. Neurosci.*, **5**, 218–228.
Munoz, D.P. & Wurtz, R.H. (1995) Saccade-related activity in monkey superior colliculus. I. Characteristics of burst and buildup cells. *J. Neurophysiol.*, **73**, 2313–2333.
Munoz, D.P., Pelisson, D. & Guitton, D. (1991a) Movement of neural activity on the superior colliculus motor map during gaze shifts. *Science*, **251**, 1358–1360.
Munoz, D.P., Guitton, D. & Pélisson, D. (1991b) Control of orienting gaze shifts by the tectoreticulospinal system in the head-free cat. III. Spatiotemporal characteristics of phasic motor discharges. *J. Neurophysiol.*, **66**, 1642–1666.
Nagy, B. & Corneil, B.D. (2010) Representation of horizontal head-on-body position in the primate superior colliculus. *J. Neurophysiol.*, **103**, 858–874.
Optican, L.M. & Robinson, D.A. (1980) Cerebellar-dependent adaptive control of primate saccadic system. *J. Neurophysiol.*, **44**, 1058–1076.
Patel, G.H., Kaplan, D.M. & Snyder, L.H. (2014) Topographic organization in the brain: searching for general principles. *Trends Cogn. Sci.*, **18**, 351–363.
Platt, M.L. & Glimcher, P.W. (1998) Response fields of intraparietal neurons quantified with multiple saccadic targets. *Exp. Brain Res.*, **121**, 65–75.
Pouget, A. & Snyder, L.W. (2000) Computational approaches to sensorimotor transformations. *Nat. Neurosci.*, **3**, 1192–1198.
Quaia, C., Lefevre, P. & Optican, L.M. (1999) Model of the control of saccades by superior colliculus and cerebellum. *J. Neurophysiol.*, **82**, 999–1018.
Quessy, S., Quinet, J. & Freedman, E.G. (2010) The locus of motor activity in the superior colliculus of the rhesus monkey is unaltered during saccadic adaptation. *J. Neurosci.*, **30**, 14235–14244.
Rezvani, S. & Corneil, B.D. (2008) Recruitment of a head-turning synergy by low-frequency activity in the primate superior colliculus. *J. Neurophysiol.*, **100**, 397–411.
Robinson, D.A. (1973) Models of the saccadic eye movement control system. *Kybernetik*, **14**, 71–83.
Rodgers, C., Munoz, D., Scott, S. & Pare, M. (2006) Discharge properties of monkey tectoreticular neurons. *J. Neurophysiol.*, **95**, 3502–3511.
Roucoux, A., Guitton, D. & Crommelinck, M. (1980) Stimulation of the superior colliculus in the alert cat. II. Eye and head movements evoked when the head is unrestrained. *Exp. Brain Res.*, **39**, 75–85.
Sajad, A., Sadeh, M., Keith, G.P., Yan, X., Wang, H. & Crawford, J.D. (2014) Visual–motor transformations within frontal eye fields during head-unrestrained gaze shifts in the monkey. *Cereb. Cortex*, **25**, 3932–3952.
Schiller, P.H. (1977) The effect of superior colliculus ablation on saccades elicted by cortical stimulation. *Brain Res.*, **122**, 154–156.
Schiller, P.H. & Wurtz, R.H. (1975) Sensorimotor transformation in the tectum of the macaque. *Neurosci. Res. Prog. B.*, **13**, 226–228.
Shen, K., Valero, J., Day, G.S. & Paré, M. (2003) Investigating the role of the superior colliculus in active vision with the visual search paradigm. *Eur. J. Neurosci.*, **33**, 2003–2016.
Smith, M.A. & Crawford, J.D. (2005) Distributed population mechanism for the 3-D oculomotor reference frame transformation. *J. Neurophysiol.*, **93**, 1742–1761.
Snyder, L.H. (2000) Coordinate transformations for eye and arm movements in the brain. *Curr. Opin. Neurobiol.*, **10**, 747–754.
Soetedjo, R., Kaneko, C.R.S. & Fuchs, A.F. (2002) Evidence that the superior colliculus participates in the feedback control of saccadic eye movements. *J. Neurophysiol.*, **87**, 679–695.
Sommer, M.A. & Wurtz, R.H. (2000) Composition and topographic organization of signals sent from the frontal eye field to the superior colliculus. *J. Neurophysiol.*, **83**, 1979–2001.
Sparks, D.L. (1975) Response properties of eye movement-related neurons in the monkey superior colliculus. *Brain Res.*, **90**, 147–152.
Sparks, D.L. (1978) Functional properties of neurons in the monkey superior colliculus: coupling of neuronal activity and saccade onset. *Brain Res.*, **156**, 1–16.
Sparks, D.L. (1986) Translation of sensory signals into commands for control of saccadic eye movements: role of primate superior colliculus. *Physiol. Rev.*, **66**, 118–171.
Sparks, D.L. (1988) Saccadic command signals in the superior colliculus: implications for sensorimotor transformations. *Can. J. Physiol. Pharm.*, **66**, 527–531.
Sparks, D.L. (1989) The neural encoding of the location of targets for saccadic eye movements. *J. Exp. Biol.*, **146**, 195–207.
Sparks, D.L. (2002) The brainstem control of saccadic eye movements. *Nat. Rev. Neurosci.*, **3**, 952–964.
Sparks, D.L. & Hartwich-Young, R. (1989) The deep layers of the superior colliculus. *Rev. Oculomot. Res.*, **3**, 213–255.
Sparks, D.L. & Mays, L.E. (1990) Signal transformations required for the generation of saccadic eye movements. *Annu. Rev. Neurosci.*, **13**, 309–336.
Stanford, T.R. & Sparks, D.L. (1994) Systematic errors for saccades to remembered targets: evidence for a dissociation between saccade metrics and activity in the superior colliculus. *Vision Res.*, **34**, 93–106.
Straube, A., Deubel, H., Ditterich, J. & Eggert, T. (2001) Cerebellar lesions impair rapid saccade amplitude adaptation. *Neurology*, **57**, 2105–2108.
Straumann, D., Zee, D.S. & Solomon, D. (2000) Three-dimensional kinematics of ocular drift in humans with cerebellar atrophy. *J. Neurophysiol.*, **83**, 1125–1140.
Stuphorn, V. (2007) New functions for an old structure: superior colliculus and head-only movements. Focus on 'the role of primate superior colliculus in the control of head movements'. *J. Neurophysiol.*, **98**, 1847–1848.
Takeichi, N., Kaneko, C.R. & Fuchs, A.F. (2007) Activity changes in monkey superior colliculus during saccade adaptation. *J. Neurophysiol.*, **97**, 4096–4107.
Van Opstal, A.J., Hepp, K., Hess, B.J., Straumann, D. & Henn, V. (1991) Two- rather than three-dimensional representation of saccades in monkey superior colliculus. *Science*, **252**, 1313–1315.
Van Opstal, A.J., Hepp, K., Suzuki, Y. & Henn, V. (1995) Influence of eye position on activity in monkey superior colliculus. *J. Neurophysiol.*, **74**, 1593–1610.
Van Opstal, J., Hepp, K., Suzuki, Y. & Henn, V. (1996) Role of monkey nucleus reticularis tegmenti pontis in the stabilization of Listing's plane. *J. Neurosci.*, **16**, 7284–7296.
Walton, M.M., Bechara, B. & Gandhi, N.J. (2007) Role of the primate superior colliculus in the control of head movements. *J. Neurophysiol.*, **98**, 2022–2037.
Wimmer, K., Nykamp, D.Q., Constantinidis, C. & Compte, A. (2014) Bump attractor dynamics in prefrontal cortex explains behavioral precision in spatial working memory. *Nat. Neurosci.*, **17**, 431–439.
Wurtz, R.H. & Albano, J.E. (1980) Visual-motor function of the primate superior colliculus. *Annu. Rev. Neurosci.*, **3**, 189–226.
Wurtz, R.H. & Goldberg, M.E. (1971) Superior colliculus cell responses related to eye movements in awake monkeys. *Science*, **171**, 82–84.
Wurtz, R.H. & Goldberg, M.E. (1972a) Activity of superior colliculus in behaving monkey. 3. Cells discharging before eye movements. *J. Neurophysiol.*, **35**, 575–586.
Wurtz, R.H. & Goldberg, M.E. (1972b) The role of the superior colliculus in visually-evoked eye movements. *Bibl. Ophthalmol.*, **82**, 149–158.
Wurtz, R.H. & Sommer, M.A. (2004) Identifying corollary discharges for movement in the primate brain. *Progress in Brain Research*, **144**, 47–60.
Wurtz, R.H., Sommer, M.A., Paré, M. & Ferraina, S. (2001) Signal transformations from cerebral cortex to superior colliculus for the generation of saccades. *Vision Res.*, **41**, 3399–3412.
Yasui, Y., Tsumori, T., Ando, A., Domoto, T., Kayahara, T. & Nakano, K. (1994) Descending projections from the superior colliculus to the reticular formation around the motor trigeminal nucleus and the parvicellular reticular formation of the medulla oblongata in the rat. *Brain Res.*, **656**, 420–426.
Zhang, M. & Barash, S. (2000) Neuronal switching of sensorimotor transformations for antisaccades. *Nature*, **408**, 971–975.